Highlights

The hydrodynamic performance of a shore-based oscillating water column device under random wave conditions

Ayrton Alfonso Medina Rodríguez,Gregorio Posada Vanegas,Beatriz Edith Vega Serratos,Itxaso Oderiz Martinez,Edgar Mendoza,Jesús María Blanco Ilzarbe,Vallam Sundar,Rodolfo Silva

- The hydrodynamic performance of the OWC device increases with the water depth leading to an increase in the pressures on its walls.
- The study highlights the dependency of amplification of the waves within the OWC chamber on the wave direction.
- The air pressure inside the chamber that dictates the efficiency of the OWC is a function of incident wave height.
- The hydrodynamic performance of the OWC in a random wave field is less than when exposed in a regular wave field.

The hydrodynamic performance of a shore-based oscillating water column device under random wave conditions

Ayrton Alfonso Medina Rodríguez[a,*], Gregorio Posada Vanegas[b], Beatriz Edith Vega Serratos[b], Itxaso Oderiz Martinez[c], Edgar Mendoza[a], Jesús María Blanco Ilzarbe[d], Vallam Sundar[e] and Rodolfo Silva[a]

[a]*Instituto de Ingeniería, Universidad Nacional Autónoma de México, Circuito Escolar, 04510, Mexico City, Mexico*
[b]*Instituto EPOMEX, Universidad Autónoma de Campeche, Av. Héroe de Nacozari 480, 24079, Campeche, Mexico*
[c]*IHCantabria - Instituto de Hidráulica Ambiental de la Universidad de Cantabria, Isabel Torres 15, 39011, Santander, Spain*
[d]*Departamento de Ingeniería Energética, Facultad de Ingeniería de Bilbao-UPV/EHU, Plaza Ingeniero Torres Quevedo, 1, 48013, Bilbao, Spain*
[e]*Department of Ocean Engineering, Indian Institute of Technology Madras, India*

ARTICLE INFO

Keywords:
Oscillating water column
Experimental tests
Irregular waves
Oblique waves
Hydrodynamic efficiency

ABSTRACT

The testing of scale models is crucial if we are to continue the development of wave energy converters. Investigations have examined the interaction of shore-based Oscillating Water Column (OWC) devices with regular water waves that impact the device perpendicularly in flumes or wave basins. However, these simplistic experiments might misrepresent the effectiveness of an OWC system. This study examines the interaction of irregular, oblique, water waves with a shore-based OWC device in terms of its hydrodynamic performance. In a spectral wave basin, a series of experiments were performed on a scale model of a single chamber of the Mutriku Wave Energy Plant. Wave propagation conditions were examined to see their impact on the hydrodynamic performance of a fixed OWC system. The wave amplification factor, hydrodynamic efficiency, non-dimensional air pressure inside the chamber, and non-dimensional water pressures on the chamber walls were evaluated. The results show that when the free surface is close to the front wall lip, the hydrodynamic efficiency increases, while the effect of significant wave height was seen to be more important in the wave amplification. Finally, it was found that the hydrodynamic efficiency under random waves is lower than that in experiments under regular waves reported previously.

1. Introduction

Wave energy has enormous potential, with the capacity to provide about twice the present annual global energy consumption (Terrero González et al., 2021). Among its different advantages is that, as compared to other renewable energy sources, it delivers a constant energy supply and its time variability of energy delivery can be more reliably predicted. However, despite its numerous benefits and the fact that the first device designs were proposed over a century ago (Ringwood, 2020), wave energy is not yet commercially viable.

Since the first registered patent for a wave energy converter (WEC) in 1898, more than a thousand ideas have been registered and this number continues to grow (McCormick, 2013; Falcão, 2010). Among the various systems that have been designed and deployed (a comprehensive overview of existing concepts and designs is available in Falcão (2010); Falnes (2007); Guedes Soares et al. (2012); Sundar et al. (2010)), the Oscillating Water Column (OWC) system has proven to be one of the most promising due to its versatility (Heath, 2012; Delmonte et al., 2016; Falcão and Henriques, 2016). An OWC device is primarily an air chamber, a turbine, valves, ducts and an electric generator. Its working principle is relatively simple: incident waves cause water to flow into the chamber through an entrance below the partially submerged front wall. The vertical free water surface oscillation inside the chamber induces the trapped air to rise and fall. This activates a two-direction turbine in a duct linked to the atmosphere. The electric generator is

*Corresponding author
ayrtonamedinar@gmail.com (A.A. Medina Rodríguez); gposadav@uacam.mx (G. Posada Vanegas); beaevega@uacam.mx (B.E. Vega Serratos); itxaso.oderiz@unican.es (I. Oderiz Martinez); emendozab@iingen.unam.mx (E. Mendoza); jesusmaria.blanco@ehu.eus (J.M. Blanco Ilzarbe); vsundar@iitm.ac.in (V. Sundar); RSilvaC@iingen.unam.mx (R. Silva)
ORCID(s): 0000-0002-0666-9472 (A.A. Medina Rodríguez); 0000-0002-0795-7759 (G. Posada Vanegas); 0000-0002-7709-1807 (B.E. Vega Serratos); 0000-0002-1991-4721 (E. Mendoza); 0000-0003-0191-2063 (J.M. Blanco Ilzarbe); 0000-0001-7421-0543 (V. Sundar); 0000-0003-0064-9558 (R. Silva)

connected to the turbine's axis to convert mechanical energy into electrical energy. Herein, the advantage is that all the moving parts of the system including the turbine are above the water surface, making maintenance easier.

To encourage the use of OWC devices, research is needed to improve existing designs and thus develop resilient, efficient devices. Regarding land-based OWC devices, which are the focus of this work, several studies have been carried out to further understand their hydrodynamic aspects numerically and experimentally (Morris-Thomas et al., 2006; Ning et al., 2016; Tsai et al., 2018; Wang et al., 2018; Torre-Enciso et al., 2009; López et al., 2016, 2019, 2020a; Daniel Raj et al., 2018; John Ashlin et al., 2017). In this regard, OWC systems are seen to achieve their optimal performance at resonance, which occurs when the incident wave frequency of the device location matches the natural frequency of the converter. Previous studies have reported that the natural resonance frequency of an OWC device depends on changes in its geometrical characteristics (chamber length and front wall submergence and width, see Evans and Porter (1995); Medina Rodríguez et al. (2020)) and on wave conditions (wave period and incidence wave direction, John Ashlin et al. (2016a); Medina Rodríguez et al. (2022)). Investigations into the considerable impact of the geometric properties of the OWC chamber on its efficiency include Chen et al. (2021); Ning et al. (2016); López et al. (2021); John Ashlin et al. (2016b); Medina Rodríguez et al. (2022).

To optimise the wave energy collected by the entire OWC system, the pneumatic chamber and also the damping created by the PTO, must work at optimum efficiency. Optimum PTO damping was investigated by López et al. (2014, 2015); Kamath et al. (2015); López et al. (2016); Elhanafi et al. (2016); Rezanejad et al. (2017); Çelik and Altunkaynak (2020); Viviano et al. (2016). According to López et al. (2015), the damping that the turbine induces on the system has a considerably greater impact on the capture factor than the wave conditions and the tidal level. Another important aspect is the air compressibility within the chamber (Falcão and Henriques, 2018; Viviano et al., 2018; Falcão and Henriques, 2019; López et al., 2020b). This is known to have a substantial impact on the power performance of full-sized converters, although it is generally ignored in model testing at a reduced scale.

Investigation using scale models is essential for the development of OWC systems; for example, showing how devices will operate and survive in the ocean. Physical modelling gives perhaps the most reliable source of information on the behaviour of WECs under various sea conditions. In particular, experiments in wave basins can offer modelling services of several sizes, that vary greatly in terms of set-up and physical size, while providing a realistic and accurate estimate of the physical model performance. This enables designers to verify the functioning of a particular device and also to optimise the installation process, thus lowering installation and operation costs. Moreover, by demonstrating that a device performs effectively under experimental testing conditions, the economic risk for companies and investors is reduced and acquiring grants or financial assistance for WEC installation might be simpler.

An onshore OWC device is often designed lie parallel to the coast; however, in real conditions waves coming perpendicular to the beach are uncommon. For example, the incident water waves that impact the Mutriku OWC wave power plant in Spain are often oblique (Ibarra-Berastegi et al., 2018), so a more genuine representation of real wave conditions can be made using oblique waves.

To characterise the performance of an onshore OWC device accurately, the influence of wave direction on hydrodynamic performance should be evaluated. Oblique waves can cause the free surface oscillation and air pressure distribution inside the OWC chamber to be irregular. This can produce a radiated flow both within and outside the chamber, causing vortices to form on the inner face of the front wall and decreasing free surface oscillation. Furthermore, as with other coastal structures, oblique waves can considerably reduce the wave loads on onshore OWC devices. Therefore, to assess the device performance correctly, incidence wave direction must be taken into account as it may have a substantial impact on the system's capacity to capture wave energy.

Among the several aspects that influence the hydrodynamic performance of an OWC, one that can be only examined through model experimentation in wave basins is the angle between the waves and the structure. However, although wave basins have fewer boundary limitations than wave flumes, the expense of operating these indoor facilities is substantially higher. For land-based OWC devices, limited data are available to estimate the effects of oblique waves. The vast majority of studies have assumed that incident waves propagate perpendicularly toward the land-based device, a scenario that rarely happens in practice. Therefore, more accurate physical model tests in wave basins with oblique waves are needed. In this regard, John Ashlin et al. (2016a) carried out an experimental investigation of the interaction of an array of OWCs embedded in a breakwater with oblique regular waves. The authors examined three distinct wave directions and came to the conclusion that the system's natural frequency was not affected. Recently, Medina Rodríguez et al. (2022) assessed the hydrodynamic performance of a single, land-based OWC device under oblique regular waves. Their research showed that the period at which resonance occurs falls, as the incoming wave angle increases for the OWC model, when it is a nearshore device.

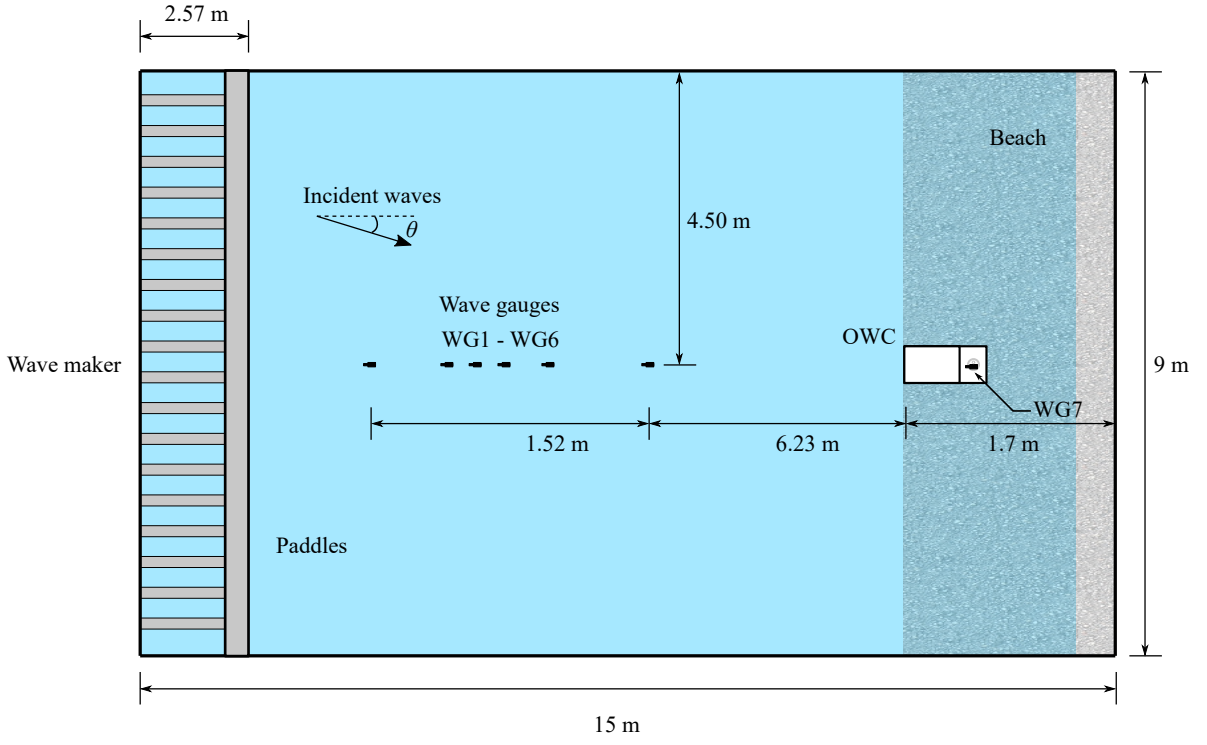

(a) Plan view of the experimental set-up.

Figure 1: Cont.

Other relevant studies of fixed OWC devices in wave basins can be found in Torre-Enciso et al. (2009); Howe and Nader (2017); John Ashlin et al. (2018); Orphin et al. (2022); Durai Eswaran et al. (2022). Orphin et al. (2022) carried out an experimental campaign in two wave basin laboratories to evaluate and compare the performance of a bottom-fixed OWC WEC under regular waves. They concluded that laboratory effects can be significant and must be taken into account in WEC model test experiments in order to improve experimental results. By causing the waves to shoal, Durai Eswaran et al. (2022) analysed the hydrodynamic performance of an OWC installed above a horizontal plate. It was stated that when the plate is present, the hydrodynamic efficiency of the OWC device increases by about 10%.

To foster the expansion of OWC technology, it is necessary to evaluate the hydrodynamic performance of OWCs under normal operating conditions. Most previous numerical and experimental studies are based on two-dimensional regular incident waves. This can give valuable information, but in the ocean, a unidirectional, regular sinusoidal wave pattern is uncommon, so the results represent an approximation of the performance of an OWC system. Thus, the objective of this work is to complement previous research in this field by evaluating the performance of a shore-based OWC WEC under oblique, irregular incident waves. A physical model of the OWC was tested in a spectral wave basin, subjected to random wave conditions, with varying peak periods, significant wave heights, water depths and wave directions.

2. Materials and methods

2.1. Experimental programme

The experiments were carried out in the 15 m-long, 9 m-wide, and 0.8 m-deep wave basin of the EPOMEX Institute at the Autonomous University of Campeche, in Mexico. The wave basin is equipped with a linear snake wave maker that produces spectral waves with 18 piston paddles, each of 50 cm width, and an active absorption system (AwaSys) (Meinert et al., 2017). An artificial gravel beach, at the other end of the basin, acted as a passive wave absorber. The

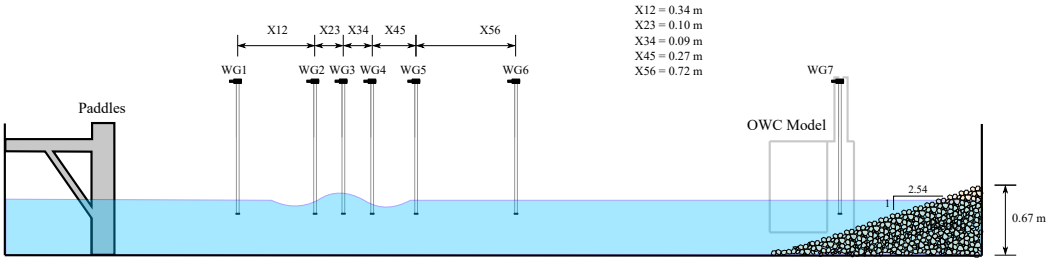

(b) Cross sectional view of the experimental set-up.

Figure 1: Schematic views of the directional wave basin and the experimental set-up (diagrams are not in scale).

mean size of the beach material was D_{50} =5.08 cm, with an average density of 2.68 g/cm^3. Schematic views of the spectral wave basin are shown in Figs. 1a and 1b.

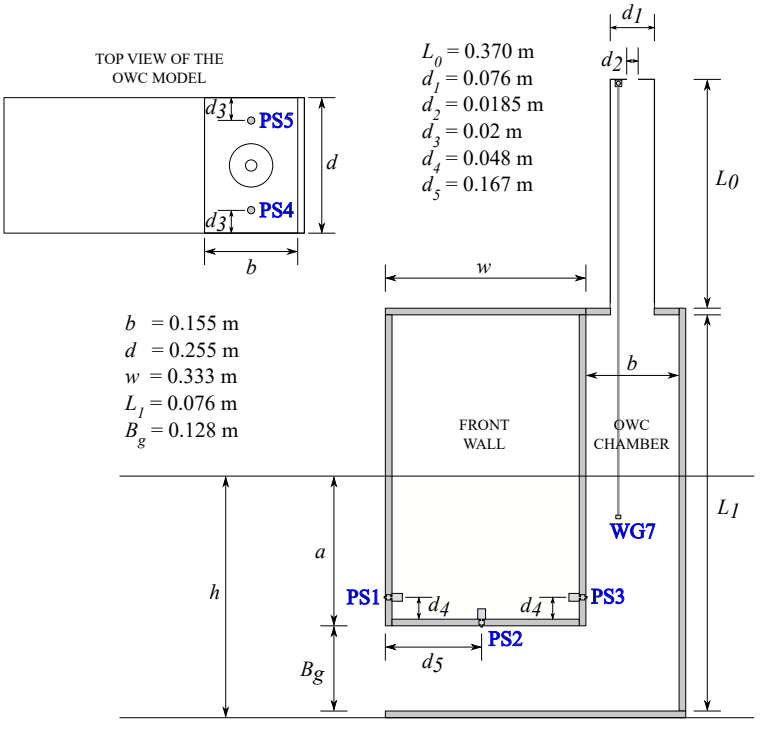

Figure 2: Vertical cross-section and dimensional details of the OWC model.

2.2. The OWC scale model

The dimensions used for the model correspond to one of the sixteen OWC chambers of the Mutriku Wave Energy Plant in Spain (Medina Rodríguez et al., 2020; Medina Rodríguez et al., 2022), as seen in Fig. 2. The model was made of 12 mm thick acrylic sheets. The length and width of the OWC chamber were b =155 mm and d =225 mm, respectively, while its height was L_1 =655 mm. The thickness of the front wall and the height of the gap below were w =260 mm and B_g =140 mm, respectively, while the front wall draft, a, and water depth, h, were varied throughout the experiments.

For modelling the OWC chamber, using the Froude similarity law, a geometric scale factor of 1:20 (1 : Λ) was

determined from the size of the experimental facilities as well as for the wave conditions and wave generation capability. Using Froude's similarity law means the model represents an analogue geometric full-scale OWC system. However, compressibility effects play an important role in OWC WECs and cannot be scaled with Froude's similarity law. These effects are seen in the aerodynamic phase, which triggers the PTO, but are minor in the hydrodynamic phase since water compressibility is low even at small scales (Payne, 2008). Falcão and Henriques (2014) proposed an alternative scale for evaluating compressibility effects, where the ratio between the volume model air chamber and the full-size device is equal to Λ^2, not Λ^3. In this case, the required capacity for the chamber is significantly more than the volume calculated with Froude similarity, and one practical solution would be to link an external reservoir with the requisite capacity to the Froude-scaled device chamber by a pipe (Sarmento, 1993). However, in this study, only the geometric similarity criterion was fully satisfied, which is a suitable way to hydrodynamically characterize the performance of an OWC in its early phases of development (López et al., 2015).

To ensure the stability of the model, four lead weights (8 kg each) were placed in the OWC chamber, as shown in Fig. 3. The PTO unit acting on the OWC system was simulated by a circular orifice to apply the equivalent resistance of a self-rectifying impulse turbine, as the line scale is too small for an accurate representation of a turbine (Falcão and Henriques, 2014). This circular orifice, at the top of the OWC chamber, has an area of χ =0.68% of the OWC chamber water plane area ($A_{owc} = b \times d$), as suggested by John Ashlin et al. (2016b).

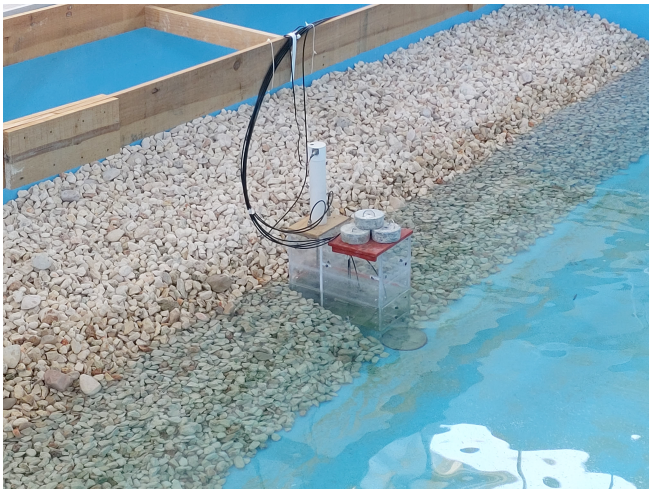

Figure 3: Experimental set-up of the shore-based OWC.

2.3. Instrumentation

To record the free surface of the water, seven resistance-type wave gauges (0.01-0.70m VTI, WG-1CH-E) were installed within the spectral wave basin. Six of these gauges (WG1-WG6) were located along the centreline of the wave basin in front of the OWC model, and the seventh, WG7, inside the scaled OWC model, as shown in Figs. 1a and 1b. Five pressure gauge sensors (0-0.3 bar Acculevel, Keller) were used, two inside the chamber, at the top, to measure the differential air pressure, and three in the front wall to record the water pressures, Fig. 2. The sampling frequency of all these sensors was 100 Hz. The differential air pressure measured by PS4 and PS5, and the chamber free surface elevation measured by WG7, were adopted to calculate the efficiency of the system, see Sections 2.7 and 2.6. The measurements were analysed inside the steady-state region of the signal.

2.4. Study site

The wave climate of Costa Azul off Ensenada, Baja California, was characterized and these random wave conditions were used to test the OWC device. In terms of wave energy, this area, the Pacific Coast of the Baja California Peninsula in northwest Mexico, is one of the most active regions of Mexico (Figs. 4a, 4b and 4c) (Fontes et al., 2019). The Costa Azul geomorphology consists of long rocky beaches and moderate-high wave power (Ventura et al., 2022). The prevailing wave systems originate from the northwestern extratropical region, though distant swells arrive from the

(a) Baja California Peninsula.

(b) Bird's eye view of Costa Azul in Ensenada.

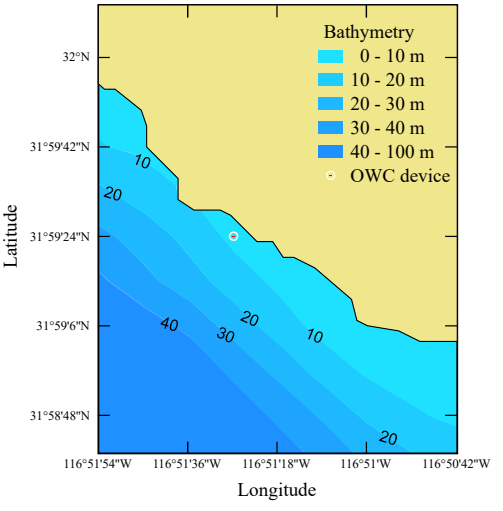

(c) Bathymetry of the proposed site (OWC device located at point 116°51'25"W,31°59'24"N, with a sea depth of approximately 7.33 m).

Figure 4: Geographical location of the study site and the proposed location for the OWC device.

Southern Hemisphere (between 180° and 315° with respect to the north) between March and November (Odériz et al., 2020). The tides are semi-diurnal mixed type, with a mean high tide of 1.61m.

The site is suitable for the installation of a shore-based OWC device as the bathymetry and wave exposure characteristics do not vary greatly (Ventura et al., 2022). There is a small port at the site, used for the supply of liquefied natural gas. This is used to generate electricity for industrial and domestic use in the municipalities of Mexicali and Rosarito, and so an OWC plant might help to accelerate the shift away from fossil fuels in the region, as well as to meet the rising demand for electricity in Baja California (Quintero-Nuñez et al., 2006). Additionally, the installation of an OWC plant with a robust front wall may help to withstand wave loads and ensure the system's survivability at this suggested study location.

To characterise the wave energy off the coast of Ensenada, the reanalysis data set of the European Centre for Medium-Range Weather Forecasts (ECMWF) ERA 5 (Hersbach et al., 2020) was used, from 1979 to 2018, with one hour and a 0.5° temporal and spatial resolutions, respectively. ERA5 uses the operational spectral wave model HRES-WAM (Günther et al., 1992), with 24 orientations and 30 frequencies. The nearest ERA5 location (117.0° W, 32.0° N), roughly 13.6 km off Costa Azul, was used for the wave data, Fig. 5. By computing the joint probability of H_{m0} and T_e, the prevailing wave conditions were obtained.

For analysing energy output in wave energy conversion, the most often occurring sea states are especially important. From Fig. 5, the most persistent sea-states (93.2% occurrence) were those with periods of 7 - 13 s, while significant

wave heights were 1.0 - 2.0 m (the dashed green square in Fig. 5). These values of the significant wave height and energy period were chosen to conduct the experimental tests and assess the OWC performance. However, it should be noted that these values are for an offshore location. Henriques et al. (2013) carried out an assessment of the transformation of the wave energy resource from an offshore to a coastal location and reported that wave power is lower and the wave period is slightly longer in coastal locations. This slight difference in wave period can have an influence on the device efficiency and cause the hydrodynamic efficiency to be overestimated. As a result, site-specific measurements should be obtained for more accurate results.

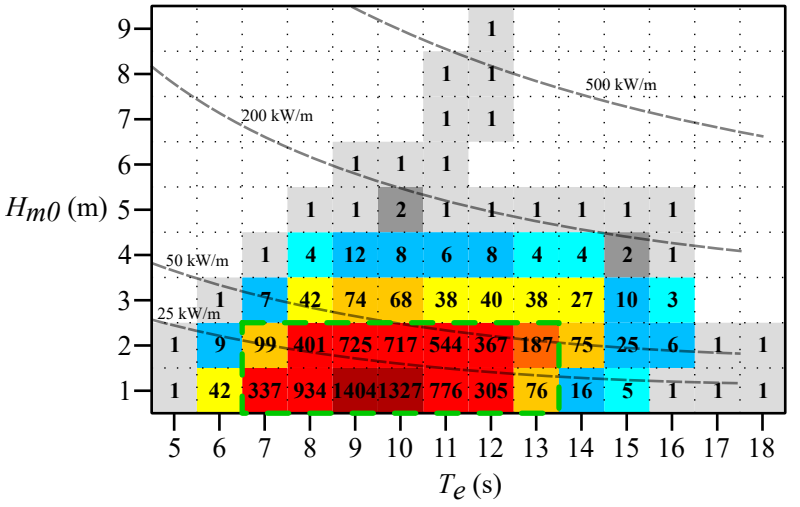

Figure 5: Characterisation of the wave resource for point 32N 117W covering the years 1979-2018 in terms of significant wave height H_{m0} and energy period T_e. The numbers represent the occurrence of sea states inside each energy bin in hours on a year, while the isolines represent wave power.

$$T_p\,(\mathrm{s}) = \begin{Bmatrix} 1.74 \\ 2.00 \\ 2.22 \\ 2.44 \\ 2.67 \\ 2.89 \\ 3.11 \\ 3.23 \end{Bmatrix} \quad H_{m0}\,(\mathrm{m}) = \begin{Bmatrix} 0.050 \\ 0.075 \\ 0.100 \end{Bmatrix} \quad h\,(\mathrm{m}) = \begin{Bmatrix} 0.30 \\ 0.40 \\ 0.50 \end{Bmatrix} \quad \theta\,(^\circ) = \begin{Bmatrix} 0 \\ 15 \end{Bmatrix}$$

Figure 6: Test wave propagating conditions covered in the experimental campaign.

2.5. Experimental wave conditions

Details of the experimental conditions are summarized in Fig. 6. A total of 144 random wave conditions were evaluated to comprehensively characterise the performance of the OWC model. These were obtained from the combination of eight peak periods: T_p =1.74 s to T_p =3.23 s, (T_p =7.78 s to T_p =14.44 s, in full-scale dimensions, or T_e =7.0 s to T_e =13.0 s with T_e = 0.90T_p (Goda, 2010; Ahn, 2021)), three significant wave heights: H_{m0} =0.050 m to H_{m0} =0.100 m, in increments of 0.025 m (H_{m0} =1.0 m to H_{m0} =2.0 m, at full-scale), three water depths: h =0.30 m to h =0.50 m, in increments of 0.10 m (h =6.0 m to h =10.0 m, in full-scale dimensions) and two incident wave angles, θ =0° and 15°. Larger wave angles were not taken into account as the lateral walls of the wave basin cause large reflections. Using the peak period as a reference, each test was designed to generate at least 200 waves. The irregular wave time series were produced using the JONSWAP spectrum (Goda, 2010), although it should be emphasised that

site-specific measurements are required to select the most accurate wave spectra, which can result in more accurate power performance data. The JONSWAP spectrum is given by

$$S(f) = \zeta H_{m0}^2 T_p^{-4} f^{-5} \exp\left[-1.25\left(T_p f\right)^{-4}\right] \gamma^{\beta}, \tag{1}$$

where T_p is the peak period, f is the wave frequency, γ is the peak enhancement factor set to 3.3, σ is the spectral shape parameter, and ζ and β are defined by the expression

$$\zeta = \frac{0.0624}{0.230 + 0.03366\gamma - 0.185\left(1.9 + \gamma\right)^{-1}}, \tag{2}$$

$$\beta = \exp\left[-\left(T_p f - 1\right)^2 / 2\sigma^2\right], \tag{3}$$

while the shape parameter is defined as

$$\sigma = \begin{cases} \sigma_a = 0.07, & \text{if} \quad f \leq f_p \\ \sigma_b = 0.09, & \text{if} \quad f > f_p \end{cases} \tag{4}$$

and where $f_p = 1/T_p$ is the peak frequency.

2.6. Dimensional Analysis

In the OWC model, the chamber characteristic (length b, width d, the thickness, draft and submerged gap of the front wall w, a and B_g, respectively), the simulated PTO (opening ratio χ), wave propagating conditions (peak period T_p, significant wave height H_{m0}, water depth h and wave direction θ), physical properties of the environment (water and air density, ρ and ρ_{air}, respectively, and gravitational acceleration g) have a strong influence on the extracted wave power (P_{out}), the amplitude of the surface displacement and the air pressure inside the chamber (η_{owc} and Δp, respectively) (He and Huang, 2016). After a first variable grouping, we obtain the following relationships

$$\left(\alpha, P_{chamber}, \epsilon\right) = f\left(\frac{a}{B_g}, \frac{d}{b}, \frac{h}{B_g}, \frac{w}{b}, \frac{H_{m0}}{B_g}, T_p\sqrt{\frac{g}{b}}, \chi, \theta\right), \tag{5}$$

where α, $P_{chamber}$ and ε are defined by

$$\alpha = \frac{\eta_{owc,m0}}{H_{m0}}, \tag{6a}$$

$$P_{chamber} = \frac{\bar{P}_{air,m0}}{\rho g B_g}, \tag{6b}$$

$$\varepsilon = \frac{P_{out}}{P_{in}}, \tag{6c}$$

where α is the wave amplification factor, $\eta_{owc,m0}$ is the calculated significant free surface elevation in the steady-state region of the signal, $P_{chamber}$ is the value of the non-dimensional air pressure within the chamber, $\bar{P}_{air,m0}$ is the average of the significant air pressures recorded by PS4 and PS5, ϵ is the hydrodynamic efficiency, while P_{in} and P_{out} represent the mean wave power of the incident waves and the average power absorbed from random waves, respectively. The parameter ϵ is used to assess the capacity of the system to transform the power of incoming waves into pneumatic power.

The dimensionless parameters d/b, w/b and χ were held constant in our experiments, while a/B_g and h/B_g are closely related to each other and therefore h/B_g is only considered. Thus, equation (5) can be reduced to

$$\left(\alpha, P_{chamber}, \epsilon\right) = f\left(\overline{h} = \frac{h}{B_g}, \overline{H} = \frac{H_{m0}}{B_g}, \overline{T} = T_p\sqrt{\frac{g}{b}}, \theta\right), \tag{7}$$

Table 1
Varying non-dimensional parameters for the experimental campaign.

Parameter	Values
Non-dimensional water depth $\left(\overline{h}\right)$	2.344, 3.125 and 3.906
Non-dimensional wave height $\left(\overline{H}\right)$	0.391, 0.586 and 0.781
Non-dimensional wave period $\left(\overline{T}\right)$	13.88, 15.91, 17.68, 19.45, 21.21, 22.98, 24.75 and 25.72
Incident wave direction (θ)	0° and 15°

and the OWC performance can be presented with only these four dimensionless parameters. Details of the values of these dimensionless parameters are given in Table 1.

Finally, the pressure exerted in the chamber by wave conditions ($\overline{h}$, $\overline{H}$, $\overline{T}$ and θ) was investigated using the following dimensionless parameters

$$P_{fwoutside} = \frac{P_{\mathrm{PS1},m0}}{\rho g B_g}, \tag{8a}$$

$$P_{fwbelow} = \frac{P_{\mathrm{PS2},m0}}{\rho g B_g} \tag{8b}$$

and

$$P_{fwinside} = \frac{P_{\mathrm{PS3},m0}}{\rho g B_g}, \tag{8c}$$

where $P_{\mathrm{PS1},m0}$, $P_{\mathrm{PS2},m0}$ and $P_{\mathrm{PS3},m0}$ are the significant water pressures recorded by PS1, PS2 and PS3, respectively.

2.7. Hydrodynamic efficiency

The hydrodynamic efficiency of the OWC device, Eq. (6c), was assessed by calculating the incident and absorbed wave power. To calculate the incident wave power, the energy spectrum of the incoming waves was estimated using data from the wave gauges. The distance between the wave paddles and wave gauge WG1 was 2.98 m and the separation between WG1 and WG2-WG6 was 0.34, 0.44, 0.53, 0.8 and 1.52 m, respectively, Fig. 1, following the least square criteria. The approach of Mansard and Funke (1980) was used to decompose the total spectrum into incoming and reflected waves induced by the OWC model and the artificial beach. Thus, the mean wave power of the incident waves, P_{in}, was computed based on the incident wave spectrum

$$P_{in} = d\rho g \int_0^{+\infty} S_i(\omega) C_g(\omega) d\omega, \tag{9}$$

where ρ is the seawater density, g is the gravitational acceleration, S_i is incident spectral density, ω is the angular frequency and C_g is the group velocity defined by

$$C_g(\omega, h) = \frac{1}{2}\frac{\omega}{k}\left(1 + \frac{2kh}{\sinh(2kh)}\right), \tag{10}$$

where k is the wave number.

On the other hand, the average power absorbed from random waves, P_{out}, can be determined by the integration of the instantaneous free surface oscillation inside the chamber moving with a velocity V_{fs} under the air pressure ΔP as follows

$$P_{out} = \frac{1}{t_e - t_i}\int_{t_i}^{t_e} \Delta P A_{owc} V_{fs} dt, \tag{11}$$

where t_i and t_e are the initial and final times, respectively, in the region of the measurements; the air pressure within the chamber ΔP is calculated by means of averaging the data gathered from the two pressure gauges (PS4 and PS5) at each time instant, and t is the time. The airflow can be assumed to be incompressible due to the small volume of air trapped inside the model (Iturrioz et al., 2015). Thus, V_{fs} can be estimated by calculating the first-time derivative of the third-order approximation to the free surface elevation inside the OWC chamber as (López et al., 2015)

$$V_{fs} = \frac{2\eta_{j+1} + 3\eta_j - 6\eta_{j-1} + \eta_{j-2}}{6\Delta t}, \tag{12}$$

where η_j is the elevation of the free surface at time t_j, j is the current time value and Δt is the sampling interval. Finally, by substituting P_{in} and P_{out}, Eqs. (9) and (11), into ε, Eq. (6c), the hydrodynamic efficiency is calculated.

3. Results and Discussion

The findings of the experiments were analysed to determine the hydrodynamic performance of the OWC chamber under random wave conditions.

3.1. Wave amplification

The wave amplification factor α is shown in Figs. 7a-7f, against non-dimensional wave period $\overline{T}$ and relative wave height $\overline{H}$ for different values of the wave angle θ and relative water depth $\overline{h}$. These figures show that most wave amplification was found for shorter, non-dimensional wave periods $\overline{T}$. This is because the excitation of the internal water column due to energy transmission from the incident waves increases Comparing the results of the left and right plots in Figs. 7a-7f, it is observed that for 0°, α increases for small and intermediate wave periods $\overline{T}$, while for the oblique case an increase in wave direction reduces the wave amplification inside the chamber for long periods ($\overline{T} > 19.45$) no matter the values of $\overline{H}$ and $\overline{h}$. This pattern may be explained by the fact that the energy entering to the chamber from incoming waves is greater when the waves approach perpendicularly to the device. As a result, the waves can excite the system without obstruction from the lateral walls of the chamber, which occurs when oblique propagation is considered. Moreover, as also explained by John Ashlin et al. (2016a), oblique wave incidence creates non-uniform excitation on the frontline of the device, which then causes uneven free surface oscillation inside the chamber. This can generate radiated flow both within and outside the chamber, causing vortices to develop on the inner face of the front wall and lowering free surface oscillation. Another aspect contributing to this finding might be oblique higher-period waves arriving first to the artificial beach, causing energy dissipation that subsequently increases as a result of the interaction with the OWC's interior and exterior walls. These two effects are also present in short-period waves; however, they are less significant since the orbital motion of fluid particles is shorter. These factors may therefore

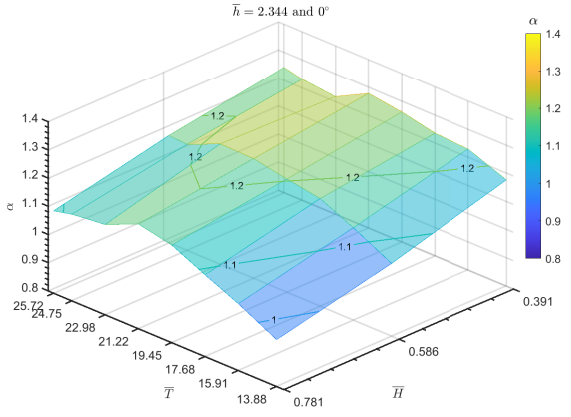

(a) α versus $\overline{T}$ and $\overline{H}$ with $\overline{h} = 2.344$ and $\theta = 0°$.

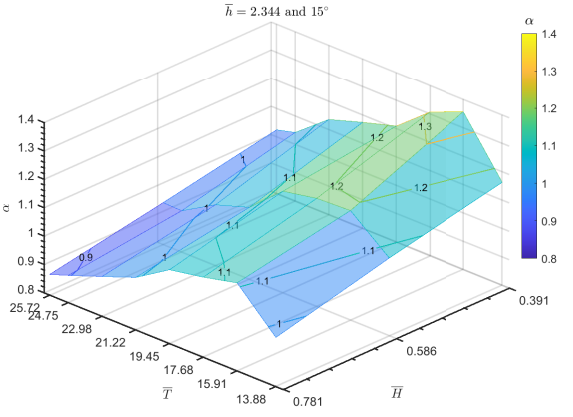

(b) α versus $\overline{T}$ and $\overline{H}$ with $\overline{h} = 2.344$ and $\theta = 15°$.

Figure 7: Cont.

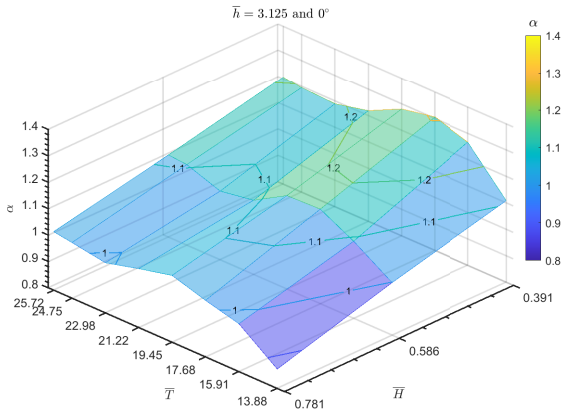

(c) α versus $\overline{T}$ and $\overline{H}$ with $\overline{h} = 3.125$ and $\theta = 0°$.

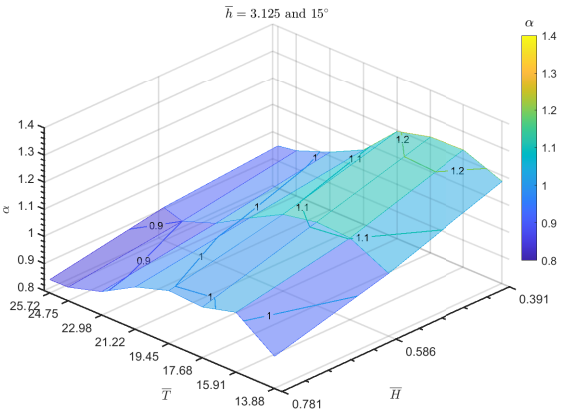

(d) α versus $\overline{T}$ and $\overline{H}$ with $\overline{h} = 3.125$ and $\theta = 15°$.

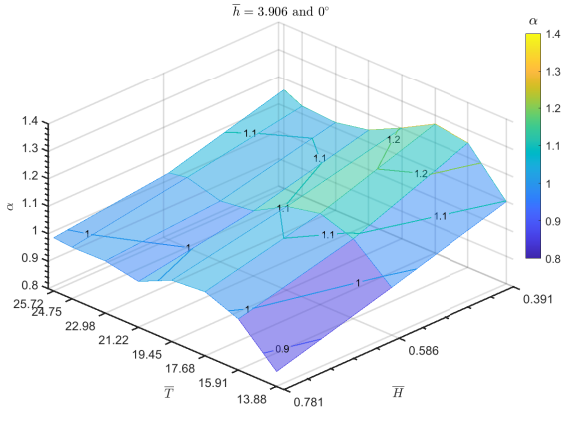

(e) α versus $\overline{T}$ and $\overline{H}$ with $\overline{h} = 3.906$ and $\theta = 0°$.

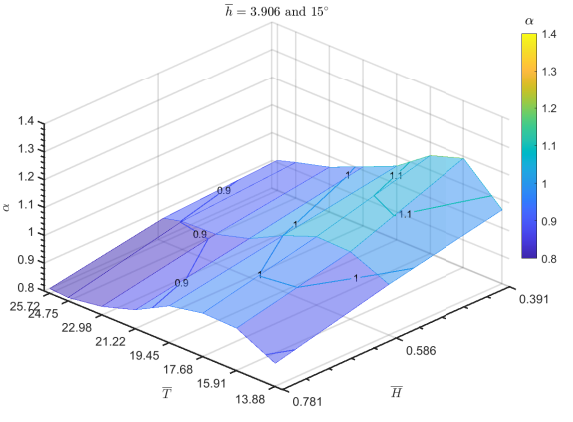

(f) α versus $\overline{T}$ and $\overline{H}$ with $\overline{h} = 3.906$ and $\theta = 15°$.

Figure 7: Amplification factor α as a function of $\overline{T}$ and $\overline{H}$ with $\theta = 0°$ and 15°.

produce a decrease in energy concentration, leading in less energy input in the chamber. On the other hand, similar to the results of Medina Rodríguez et al. (2022) for regular waves, Figs. 7a-7f show that α increases as $\overline{H}$ decreases. This is because the volume of trapped air in the upper section of the chamber decreases as the height of the water surface inside the chamber rises, this leads to an increase in the pressure and restricts the rising wave elevation in the chamber. Regarding the effect of the non-dimensional water depth $\overline{h}$, it is observed that the wave amplification inside the OWC chamber increases when $\overline{h}$ decreases. This trend could be similar to that explained above for an increase in $\overline{H}$, in this case, when $\overline{h}$ increases, the air volume decreases and leads to a constraint on the increasing wave elevation.

3.2. Non-dimensional air pressure

The results of $P_{chamber}$ against the non-dimensional peak period $\overline{T}$ and the relative wave height $\overline{H}$ are shown in Figs. 8a-8f for various incident wave angles θ and relative water depths $\overline{h}$. It is clear that $P_{chamber}$ increases as the wave height increases and the peak period decreases. This trend is due to the increasing compression of the trapped air volume caused by higher waves and shorter wavelengths, which supports the above argument, explained in subsection 3.1. The trend is also consistent with what was found by Medina Rodríguez et al. (2022) for regular waves after reaching a maximum at $\overline{T} = 14.32$, where the air pressure decreases as the wave period increases and wave height decreases. Furthermore, it can be inferred from Figs. 8a-8f that higher pressure in the short period region suggests that more energy may be transmitted across the gap into the chamber. Regarding the effect of the angle of incidence,

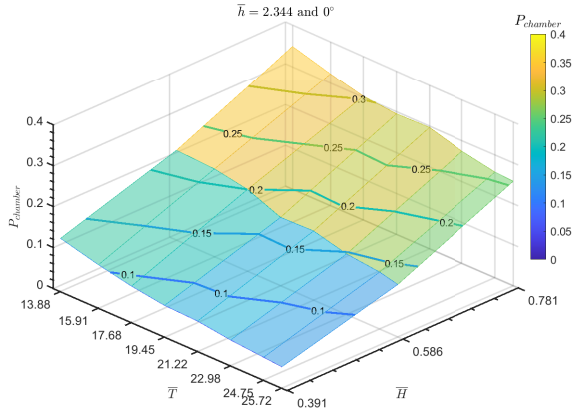

(a) $P_{chamber}$ versus $\overline{T}$ and $\overline{H}$ with $\overline{h} = 2.344$ and $\theta = 0°$.

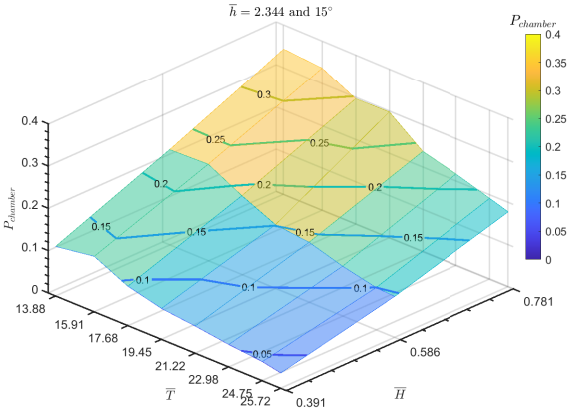

(b) $P_{chamber}$ versus $\overline{T}$ and $\overline{H}$ with $\overline{h} = 2.344$ and $\theta = 15°$.

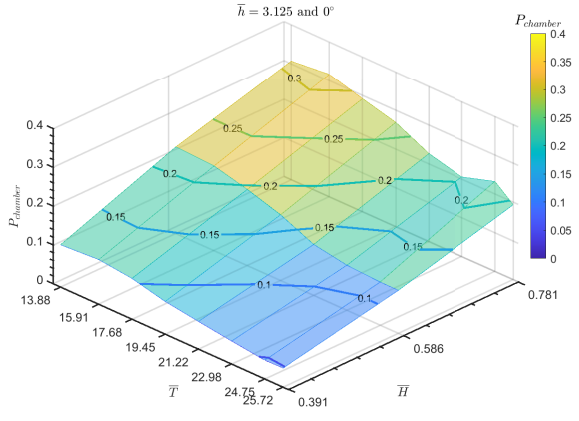

(c) $P_{chamber}$ versus $\overline{T}$ and $\overline{H}$ with $\overline{h} = 3.125$ and $\theta = 0°$.

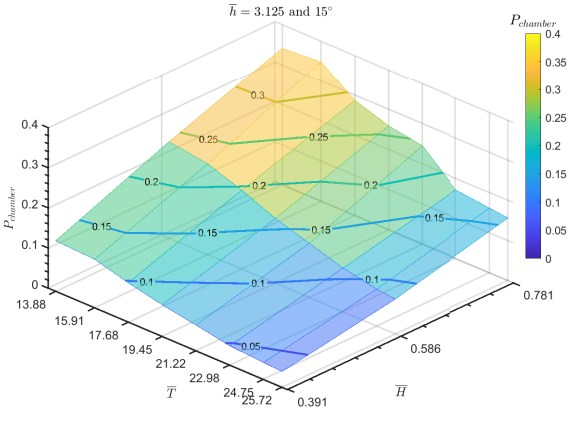

(d) $P_{chamber}$ versus $\overline{T}$ and $\overline{H}$ with $\overline{h} = 3.125$ and $\theta = 15°$.

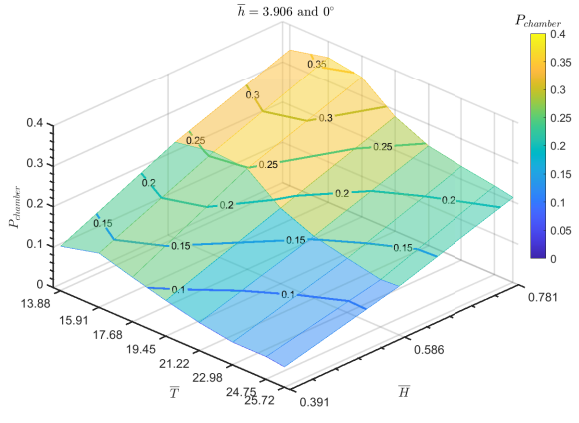

(e) $P_{chamber}$ versus $\overline{T}$ and $\overline{H}$ with $\overline{h} = 3.906$ and $\theta = 0°$.

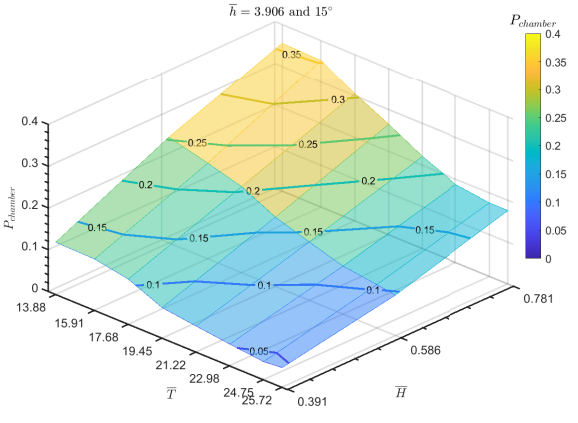

(f) $P_{chamber}$ versus $\overline{T}$ and $\overline{H}$ with $\overline{h} = 3.906$ and $\theta = 15°$.

Figure 8: Non-dimensional pressure inside the OWC chamber $P_{chamber}$ as a function of $\overline{T}$ and $\overline{H}$ with $\theta = 0°$ and 15°.

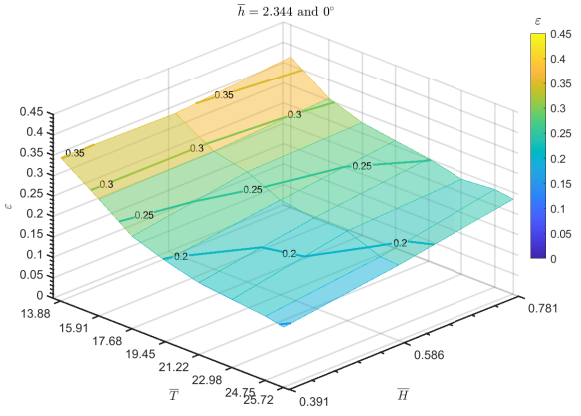

(a) ε versus $\overline{T}$ and $\overline{H}$ with $\overline{h} = 2.344$ and $\theta = 0°$.

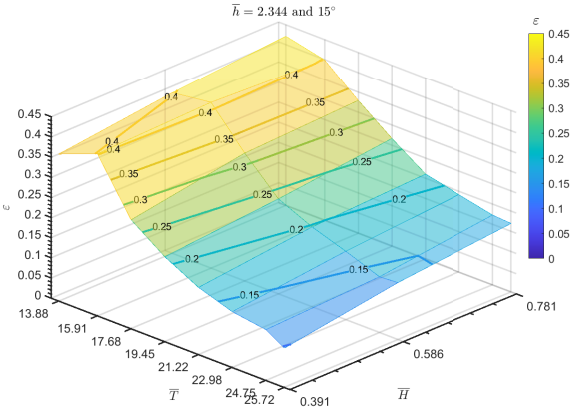

(b) ε versus $\overline{T}$ and $\overline{H}$ with $\overline{h} = 2.344$ and $\theta = 15°$.

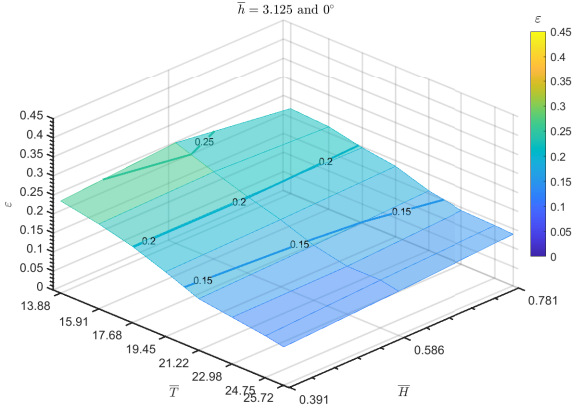

(c) ε versus $\overline{T}$ and $\overline{H}$ with $\overline{h} = 3.125$ and $\theta = 0°$.

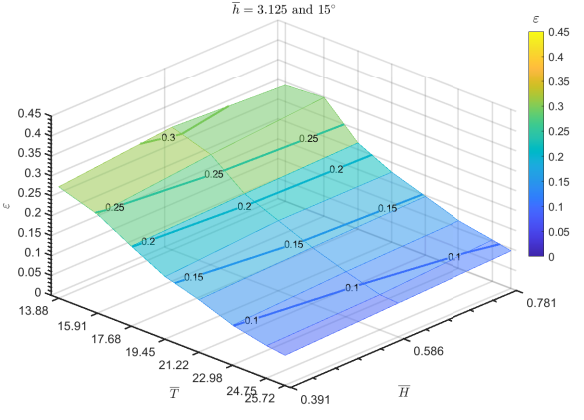

(d) ε versus $\overline{T}$ and $\overline{H}$ with $\overline{h} = 3.125$ and $\theta = 15°$.

Figure 9: Cont.

it is seen that for longer peak periods, the air pressure within the OWC chamber decreases when $\theta = 15°$, which is directly in line with the reduction in α, shown in Figs. 7a-7f. However, the results suggest that this parameter does not significantly affect the magnitude of $P_{chamber}$. On the other hand, Figs. 8e-8f show that $P_{chamber}$ increases with an increase of $\overline{h}$ at small non-dimensional peak periods, which is due to the reduction in the trapped air volume.

3.3. Hydrodynamic efficiency

Figures 9a–9f show the combined effect of $\overline{T}$ and $\overline{H}$ on ε for different water depths $\overline{h}$ and angle of incident wave θ. First, by comparing the different water depths $\overline{h}$, shown in Figs. 9a–9f, it is seen that as the non-dimensional water depth $\overline{h}$ increases, hydrodynamic efficiency is reduced. This could be explained by the fact that an increase in water depth leads to an increase in the front wall draft which reduces the energy transmission from the incoming waves to the internal water column.

In Figs 9a–9f, similar trends to that reported by Medina Rodríguez et al. (2022) regarding the effect of $\overline{T}$ are seen, since, for short peak periods that are close the resonance period of the OWC model, ε is higher, while at long periods, far from resonance, ε decreases. This may be because energy transfer is greater for shorter wave periods, resulting in both higher excitation of the internal water column and the air pressure inside the chamber. For regular waves, Medina Rodríguez et al. (2022) reported that the resonance period of the OWC model was found at $\overline{T} = 14.32$ for $\overline{h}$ =3.125. In the present results, under the water depth conditions shown in Figs. 9c–9d, it is not clear that this occurs

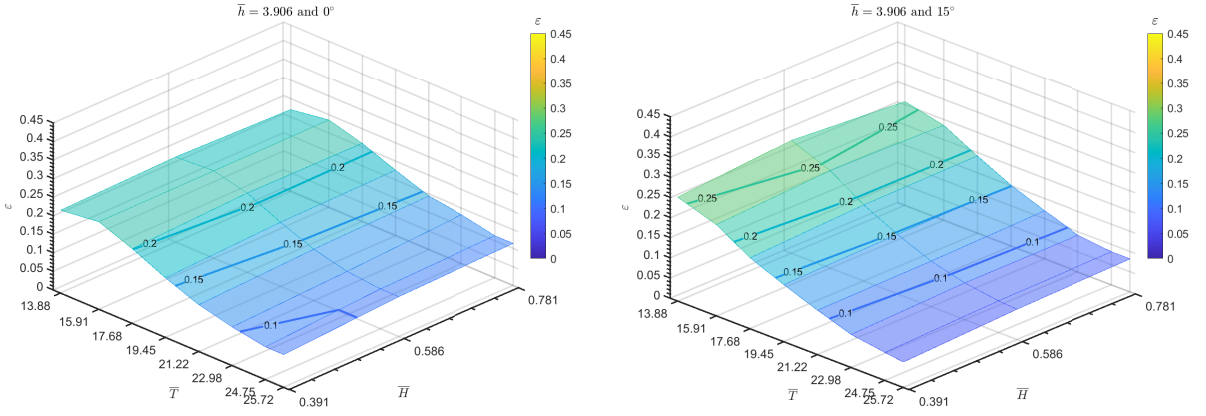

(e) ε versus $\overline{T}$ and $\overline{H}$ with $\overline{h} = 3.906$ and $\theta = 0°$.

(f) ε versus $\overline{T}$ and $\overline{H}$ with $\overline{h} = 3.906$ and $\theta = 15°$.

Figure 9: Hydrodynamic efficiency ε as a function of $\overline{T}$ and $\overline{H}$ with $\theta = 0°$ and 15°.

at a similar peak period. Furthermore, the findings shown in Figs. 9a–9f demonstrate that the effect of $\overline{H}$ on ε is less relevant the higher the magnitude of $\overline{h}$. This may be because a large front wall draft, produced by higher water depth, leads to higher energy reflection and wave energy is prevented from entering the chamber.

Furthermore, Figs. 9a–9f show that the hydrodynamic efficiency ε is influenced by the incidence wave angle θ. In Fig. 9a and 9b, it is evident that for $\overline{T}$ <19.45, ε is higher when θ increases, while for large non-dimensional wave periods the trend is reversed. This trend is similar to the wave amplification depicted in Figs. 7a-7f, and can be explained by the variation of energy entering the chamber due to wave direction and the scattering and reflection phenomena that occurs when oblique higher-period waves interact with the artificial beach and the lateral walls of the wave basin. A similar trend is observed in Figs. 9c–9d and 9e– 9f with $\overline{h}$ =3.125 and 3.096, respectively, although the variation is reduced and the magnitude of $\overline{T}$ at which the trend is reversed decreases with an increase in $\overline{h}$. In Fig. 9e a small, but pronounced peak in the hydrodynamic efficiency ε at $\overline{T} = 15.91$ for $\theta = 0°$ is seen. This could be explained by the fact that as the front wall draft increases, the distance the fluid particle must travel vertically during a period of motion increases, producing a higher wave period at which resonance occurs, than the wave period observed for regular waves ($\overline{T} = 14.32$) as mentioned above.

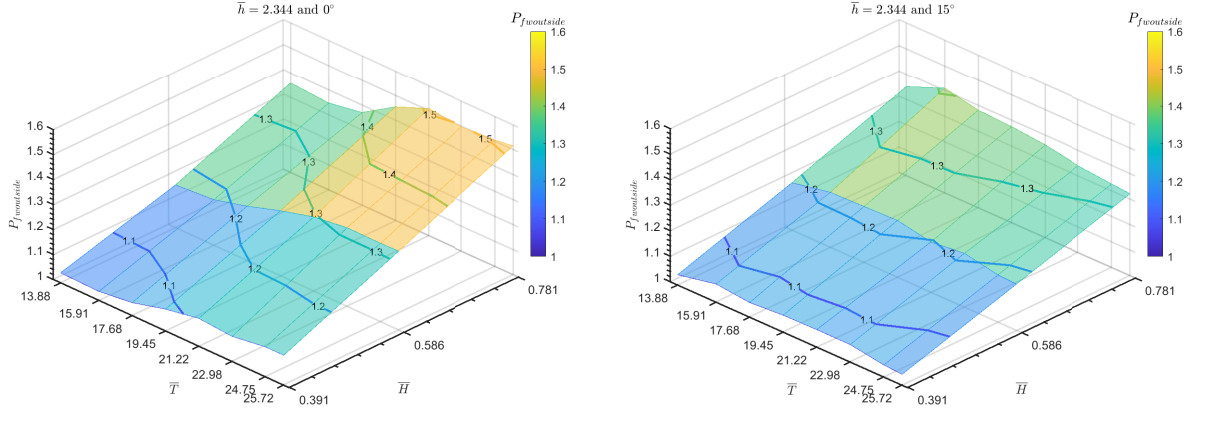

(a) $P_{fwoutside}$ versus $\overline{T}$ and $\overline{H}$ with $\overline{h} = 2.344$ and $\theta = 0°$.

(b) $P_{fwoutside}$ versus $\overline{T}$ and $\overline{H}$ with $\overline{h} = 2.344$ and $\theta = 15°$.

Figure 10: Cont.

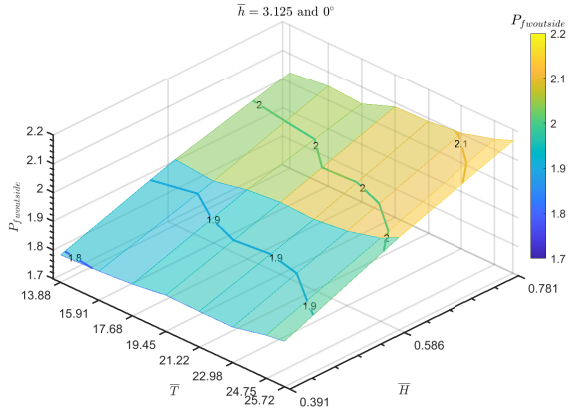

(c) $P_{fwoutside}$ versus $\overline{T}$ and $\overline{H}$ with $\overline{h} = 3.125$ and $\theta = 0°$.

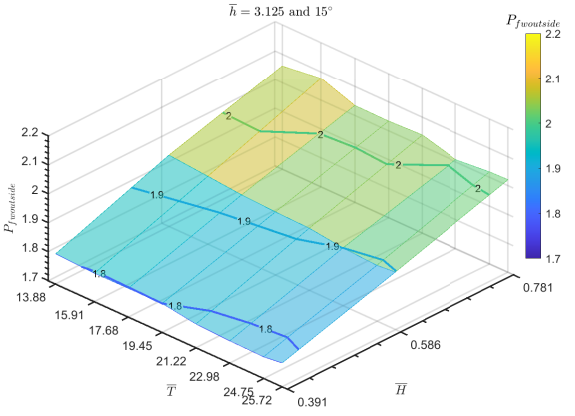

(d) $P_{fwoutside}$ versus $\overline{T}$ and $\overline{H}$ with $\overline{h} = 3.125$ and $\theta = 15°$.

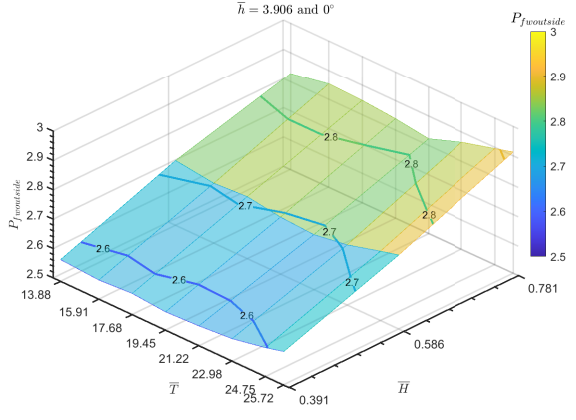

(e) $P_{fwoutside}$ versus $\overline{T}$ and $\overline{H}$ with $\overline{h} = 3.906$ and $\theta = 0°$.

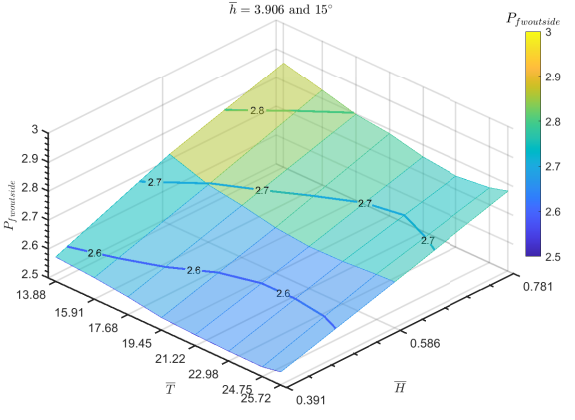

(f) $P_{fwoutside}$ versus $\overline{T}$ and $\overline{H}$ with $\overline{h} = 3.906$ and $\theta = 15°$.

Figure 10: Non-dimensional water pressure outside the chamber $P_{fwoutside}$ as a function of $\overline{T}$ and $\overline{H}$ with $\theta = 0°$ and 15°.

3.4. Non-dimensional water pressure outside the front wall

The results for $P_{fwoutside}$ versus both the non-dimensional peak period $\overline{T}$ and the relative wave height $\overline{H}$ are shown in Figs. 10a-10f for variable incidence wave angles θ and water depths $\overline{h}$. The water pressure measurements were taken near the seaward opening of the OWC chamber. The pressure at the seaward side of the front wall increases when wave height rises. This increase is higher at lower water depths, for instance for θ =0°, $P_{fwoutside}$ increases in average 15%, 7% and 5% for $\overline{h} = 2.344$, 3.125 and 3.906, respectively. Comparing the left and right plots in Figs. 10a-10f, it can be seen that water pressure outside the front wall is higher under normal wave propagation. This may be explained by the energy dissipation caused by the artificial beach and the spread of lateral energy, which both rise with the incident wave direction.

3.5. Non-dimensional water pressure below the front wall

The results of the non-dimensional water pressure below the front wall $P_{fwbelow}$ for variable wave angle of incidence θ and dimensionless peak period $\overline{T}$, water depth $\overline{h}$ and wave height $\overline{H}$ are shown in Figs. 11a–11f. In these figures, there is a clear increasing trend in $P_{fwbelow}$ when $\overline{H}$ increases. In fact, this trend is more pronounced at lower water depths. This might be explained by the fact that when incident waves interact with the front wall, the orbital motion of wave particles has a greater impact on the pressure exerted below the front wall as the draft of the front wall

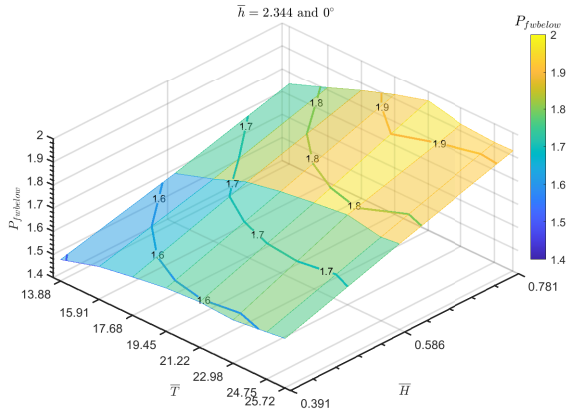

(a) $P_{fwbelow}$ versus $\overline{T}$ and $\overline{H}$ with $\overline{h} = 2.344$ and $\theta = 0°$.

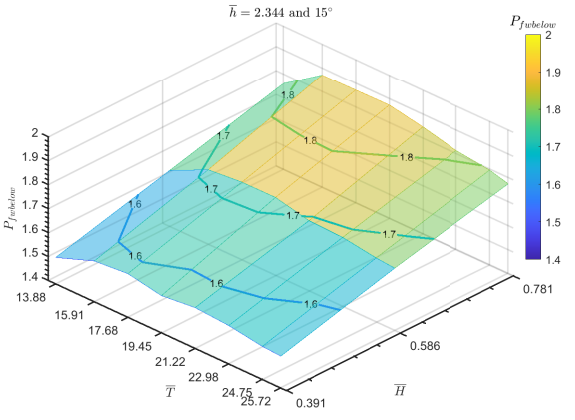

(b) $P_{fwbelow}$ versus $\overline{T}$ and $\overline{H}$ with $\overline{h} = 2.344$ and $\theta = 15°$.

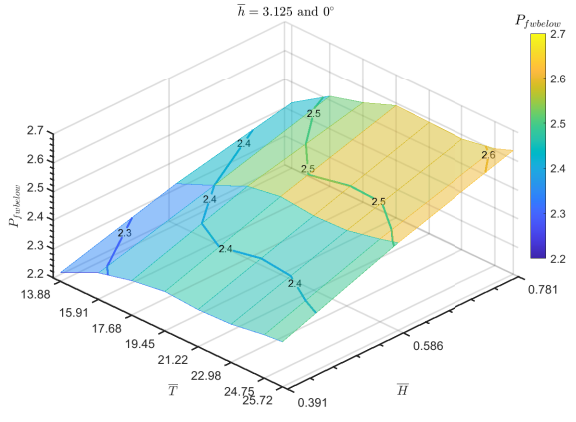

(c) $P_{fwbelow}$ versus $\overline{T}$ and $\overline{H}$ with $\overline{h} = 3.125$ and $\theta = 0°$.

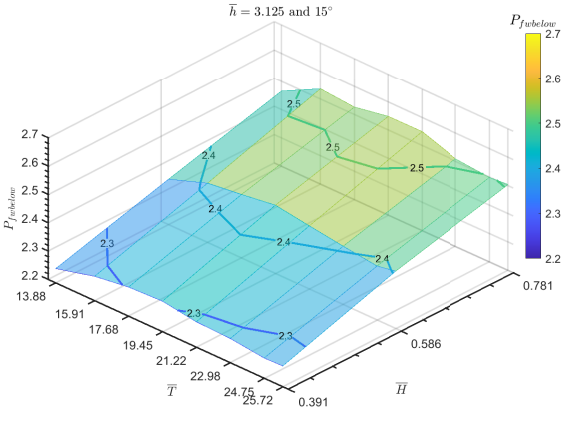

(d) $P_{fwbelow}$ versus $\overline{T}$ and $\overline{H}$ with $\overline{h} = 3.125$ and $\theta = 15°$.

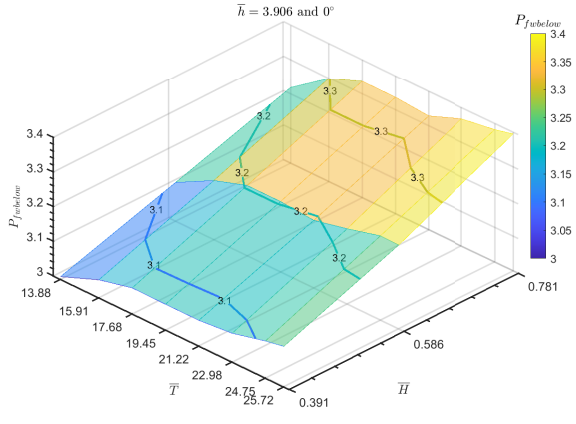

(e) $P_{fwbelow}$ versus $\overline{T}$ and $\overline{H}$ with $\overline{h} = 3.906$ and $\theta = 0°$.

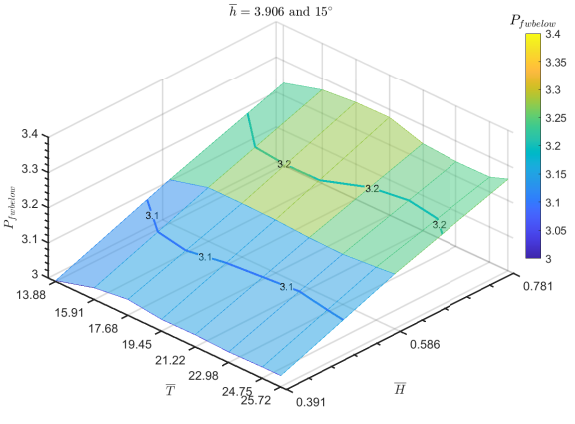

(f) $P_{fwbelow}$ versus $\overline{T}$ and $\overline{H}$ with $\overline{h} = 3.906$ and $\theta = 15°$.

Figure 11: Non-dimensional water pressure below the front wall lip $P_{fwbelow}$ as a function of $\overline{T}$ and $\overline{H}$ with $\theta = 0°$ and 15°.

becomes less and the wave height increases. For normal wave incidence, $P_{fwbelow}$ is greater as the non-dimensional peak period $\overline{T}$ increases, which means that longer waves generate higher pressures below the front wall. For oblique wave incidence, water pressure increases for intermediate values of $\overline{T}$, while for higher values of $\overline{T}$, water pressure decreases slightly again.

3.6. Non-dimensional water pressure inside the front wall

These water pressure measurements were taken at the same depth as those taken outside the front wall. The results are shown in Figs. 12a–12f, which show the variation of $P_{fwinside}$ for variable wave direction θ, dimensionless peak period $\overline{T}$, water depth $\overline{h}$ and wave height $\overline{H}$. In addition to Figs. 10a–10f and 11a–11f, from Figs. 12a to 12f it can be seen that the water pressure inside the chamber $P_{fwinside}$ follows the same trend, increasing when $\overline{H}$ increases. In the case of $P_{fwinside}$, this is due to the higher waves that generate higher pressures within the chamber. Comparing the results for normal and oblique wave incidence in Figs.12a–12f, it can be seen that $P_{fwinside}$ is higher with normal wave propagation. This is because, under oblique wave incidence, non-uniform wave amplification occurs within the device, causing irregular pressure oscillations.

In Appendix A, a table with the trends observed in subsections 3.1- 3.6 is provided.

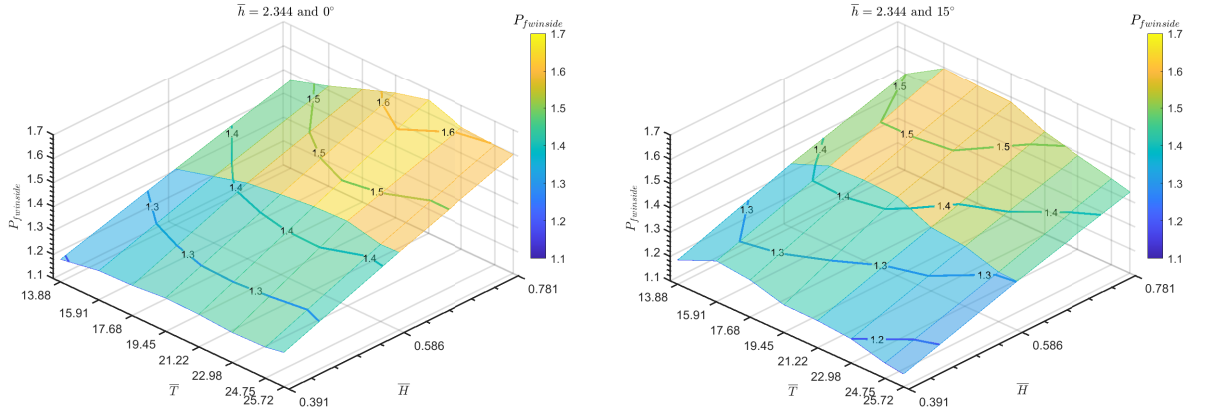

(a) $P_{fwinside}$ versus $\overline{T}$ and $\overline{H}$ with $\overline{h} = 2.344$ and $\theta = 0°$.

(b) $P_{fwinside}$ versus $\overline{T}$ and $\overline{H}$ with $\overline{h} = 2.344$ and $\theta = 15°$.

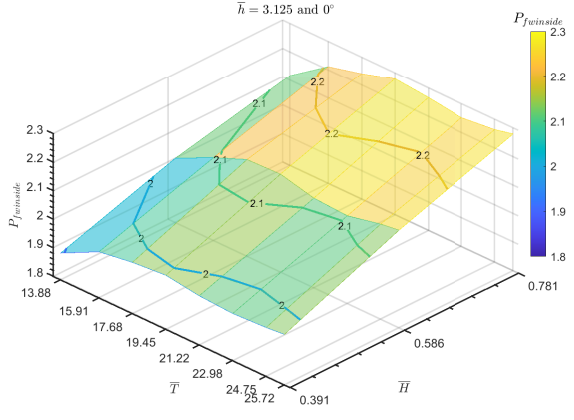

(c) $P_{fwinside}$ versus $\overline{T}$ and $\overline{H}$ with $\overline{h} = 3.125$ and $\theta = 0°$.

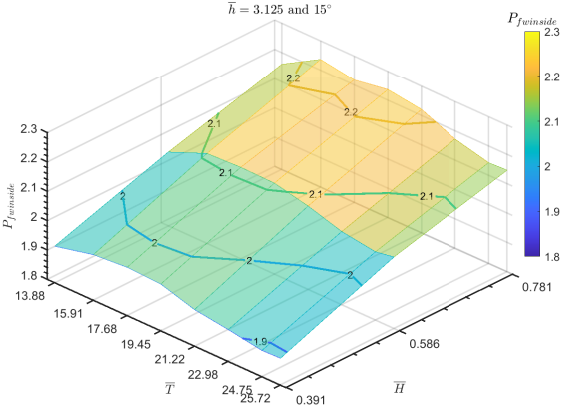

(d) $P_{fwinside}$ versus $\overline{T}$ and $\overline{H}$ with $\overline{h} = 3.125$ and $\theta = 15°$.

Figure 12: Cont.

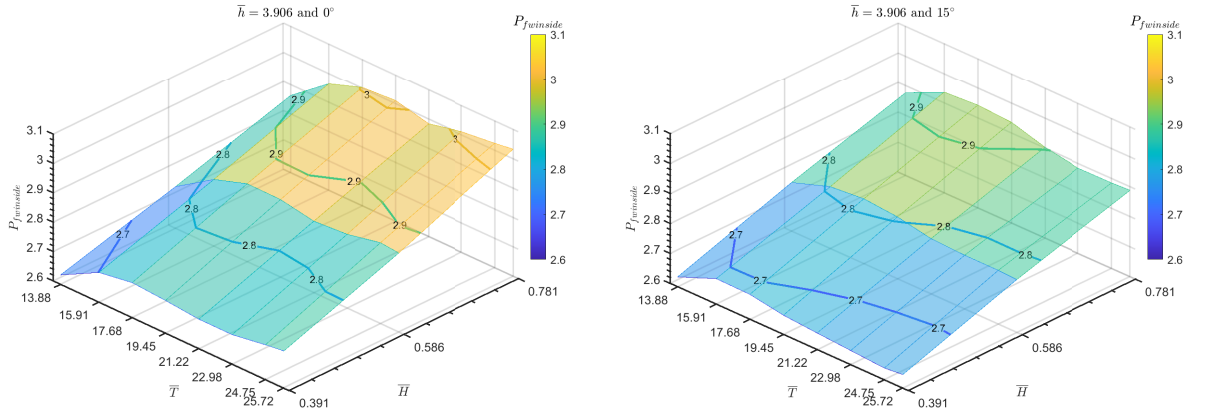

(e) $P_{fwinside}$ versus $\overline{T}$ and $\overline{H}$ with $\overline{h} = 3.906$ and $\theta = 0°$.

(f) $P_{fwinside}$ versus $\overline{T}$ and $\overline{H}$ with $\overline{h} = 3.906$ and $\theta = 15°$.

Figure 12: Non-dimensional water pressure inside the chamber $P_{fwinside}$ as a function of $\overline{T}$ and $\overline{H}$ with $\theta = 0°$ and 15°.

3.7. Comparison with regular waves

A comparison between the results reported by Medina Rodríguez et al. (2022) for regular waves and the results for random waves was made. Figs. 13a–13b show the amplification factor α and hydrodynamic efficiency ε, respectively, against $\overline{T}$ for $\theta = 0°$ and 15° and for regular and random waves. It is seen that for the longest periods the free surface amplification and the hydrodynamic efficiency for the oblique case are lower than those for normal propagation. This might be because, with oblique waves, there is more energy dissipation over the artificial beach, resulting in reduced wave amplification which means less air compression and lower power output. It can also be seen that for random waves, α and ε are lower compared to the regular case, under both normal and oblique propagation. In Fig. 13a, at their corresponding peaks, it is seen that the amplification factor α, under regular waves, is higher, approximately 66% and 71% more than that of random waves for $\theta = 0°$ and 15°, respectively. On the other hand, in Fig. 13b it is observed that for ε, the magnitude in the peaks for regular waves is around 30% greater than in the random wave case under both normal and oblique propagation. The reason for these differences can be explained by the lower free surface amplification, flow rate and air pressure within the chamber, found in irregular waves compared to regular waves. To further explain this, Figs. 14a–14b are presented, showing the time series for regular and random waves of wave elevation $\bar{\alpha}$, air pressure within the chamber $\bar{P}_{chamber}$ and flow rate $\bar{Q}$ with $\overline{T}$ =15.91, $\overline{H} = 0.781$, $\overline{h} = 3.125$ and $\theta = 0°$ are shown. The time series for random waves are presented for $T_p = 2.0$ s, while Fig. 14a shows the equivalent

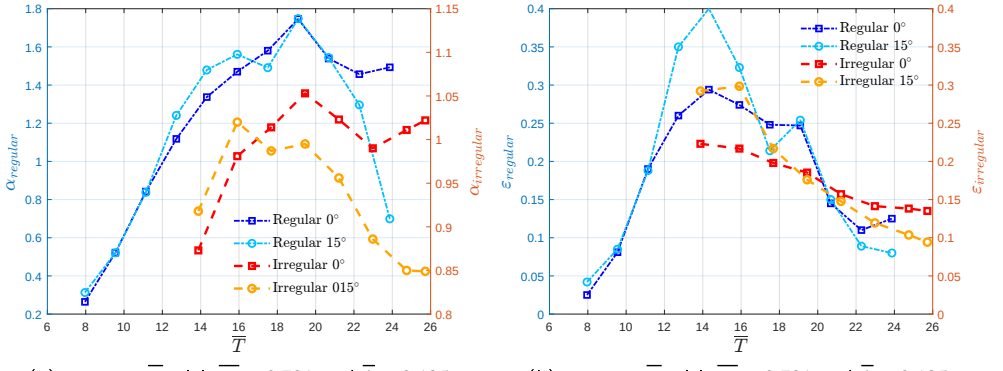

(a) α versus $\overline{T}$ with $\overline{H} = 0.781$ and $\overline{h} = 3.125$.

(b) ε versus $\overline{T}$ with $\overline{H} = 0.781$ and $\overline{h} = 3.125$.

Figure 13: Amplification factor α and hydrodynamic efficiency ε as a function of $\overline{T}$ for $\theta = 0°$ and 15° and for regular (Medina Rodríguez et al., 2022) and random waves.

regular wave with the wave period equal to the energy period in random waves ($T_e = 1.8$ s). The parameters are defined as $\bar{\alpha} = \eta_{owc}/H_{m0}$, $\bar{P}_{chamber} = \bar{P}_{air}/\rho g B_g$ and $\bar{Q} = V_{fs}/\left(H_{m0} 2\pi/T_p\right)$, where η_{owc} and $\bar{P}_{air}$ are the time variation of free surface elevation and average air pressure inside the chamber. In Fig. 14a, it can be seen that the wave pattern in $\bar{\alpha}$ is uniform and sinusoidal, and as a consequence, the flow rate $\bar{Q}$ and air pressure $\bar{P}_{chamber}$ are similar, while in Fig. 14b the wave patterns are irregular and are smaller in magnitude. In general, their amplitudes and phases are very important, since the hydrodynamic efficiency is determined by P_{out} which is calculated using Eq. 11. In this equation, P_{out} is the instantaneous integration of the product between the air pressure and flow rate; the smaller their product, the lower the average power absorbed and efficiency for random waves. Therefore, the location of a shore-based OWC may be as important as the offshore wave conditions, owing to the local interactions of waves with the sea bed and coastal contours that filter and modify the wave energy as these waves reach the shore.

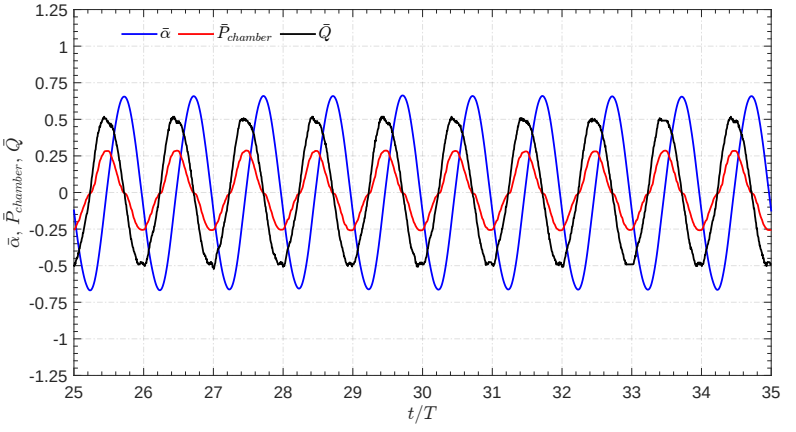

(a) Time series of $\bar{\alpha}$, $\bar{P}_{chamber}$ and $\bar{Q}$ for regular waves (Medina Rodríguez et al., 2022).

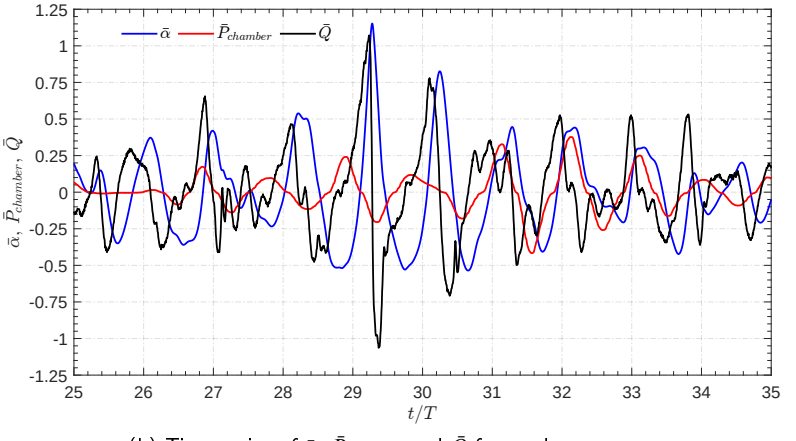

(b) Time series of $\bar{\alpha}$, $\bar{P}_{chamber}$ and $\bar{Q}$ for random waves.

Figure 14: Time series of wave elevation $\bar{\alpha}$, air pressure within the chamber $\bar{P}_{chamber}$ and volume flow rate $\bar{Q}$ with $\overline{T}$ =15.91, $\overline{H} = 0.781$, $\overline{h} = 3.125$ and $\theta = 0°$ for regular (Medina Rodríguez et al., 2022) and random waves.

4. Conclusions

The hydrodynamic performance of a shore-based OWC-WEC was investigated through a series of tests under random wave conditions. The investigation explored the influence of wave propagating conditions, such as significant wave height, peak period, incident direction and water depth, on the wave amplification factor, hydrodynamic efficiency, and water and air pressures. Overall, the variation patterns of the measured air pressure within the chamber and the hydrodynamic efficiency agree well with previously published results for regular waves.

Table 2
Trends observed in the experiments (↑ indicates an increase while ↓ indicates a decrease).

Parameter	$\overline{H}$	$\overline{T}$	$\overline{h}$	θ
α	↑ when $\overline{H}$ ↓	No linear relation	↑ when $\overline{h}$ ↓	No linear relation
ε	No linear relation	↑ when $\overline{T}$ ↓	↑ when $\overline{h}$ ↓	No linear relation
$P_{chamber}$	↑ when $\overline{H}$ ↑	↑ when $\overline{T}$ ↓	No linear relation	No linear relation
$P_{fwoutside}$	↑ when $\overline{H}$ ↑	No linear relation	↑ when $\overline{h}$ ↑	No linear relation
$P_{fwbelow}$	↑ when $\overline{H}$ ↑	No linear relation	↑ when $\overline{h}$ ↑	No linear relation
$P_{fwinside}$	↑ when $\overline{H}$ ↑	No linear relation	↑ when $\overline{h}$ ↑	No linear relation

For different wave heights, the amplification inside the chamber was seen to have similar trends to those previously observed for regular waves (Medina Rodríguez et al., 2022). It was found that the amplification decreases as the wave height and water depth increase. Regarding the air pressure within the chamber, it was found that this is higher for short peak periods and large wave heights. However, no significant difference was seen between the air pressure results for normal and oblique propagation.

The water pressures outside, below and inside the front wall of the device increase when wave height increases. These water pressures are also found to decrease slightly under oblique wave propagation. A positive correlation was also found between the increase in the water pressures and a higher water depth.

For hydrodynamic efficiency, the results show that this falls when the front wall draft is greater due to an increase in water depth. This finding is significant, as it infers that energy transmission from the incoming waves to the internal water column is less when there is a greater front wall draft. Small differences in hydrodynamic efficiency were found for normal and oblique propagation, which may be due to the energy dissipation caused by the artificial beach that dissipates part of the incident energy. On the other hand, it was seen that significant wave height has a slight effect on the efficiency, being more crucial for lower depths of water.

The present findings on efficiency show significant differences from those previously published for regular waves (Medina Rodríguez et al., 2022). The hydrodynamic efficiency from random waves was found to be lower than that in regular waves for similar wave conditions. For this reason, testing under random waves is important and may provide a more accurate assessment of their influence on the device's performance in real sea conditions.

It is worth noting that if an OWC plant is to be installed in Costa Azul, prior monitoring of the wave climate is required. As previously stated, the sea states used in this study are for deep waters where the wave motion is undisturbed by the bottom. Shoaling and refraction are two of the most important phenomena to consider as waves approach the shore because they can affect wave periods and heights, and hence the flux of wave energy available. The performance of the OWC device is also significantly affected by tidal variation, as shown in the present results, and thus it should also be examined. Furthermore, although the OWC plant in Mutriku provided the model dimensions used in this study, alternative chamber designs could be more suitable for the wave climate of Costa Azul.

Finally, it is hoped that this experimental work may be useful in future research on the impact of wave propagation conditions on the hydrodynamic performance of OWCs. Future studies in wave basins could investigate the influence of the PTO and the use of an additional air reservoir to improve the ratio of inertia forces to air compression forces (Sarmento, 1993). The model may then be expanded to cover a group of OWC systems that will allow more energy to be produced.

A. Trends observed in the results

In Table 2 gives a summary of the trends observed in the results section. For all four wave propagating condition variables (non-dimensional wave height, peak period, water depth and wave direction) whether the outcome increases, decreases or no linear relation was observed within the range of the parameters considered is shown. In this table it can be seen that a modification in the non-dimensional wave height and water depth has a linear relation with most of the hydrodynamic parameters, while for the non-dimensional peak period it was only observed with the hydrodynamic efficiency and wave amplification. However, a variation of the wave direction did not show a linear relation with any of the hydrodynamic parameters.

CRediT authorship contribution statement

Ayrton Alfonso Medina Rodríguez: Conceptualization of this study, Methodology, Software, Validation, Formal analysis, Investigation, Data curation, Writing - Original draft preparation, Writing - Review and editing, Visualization. **Gregorio Posada Vanegas:** Conceptualization, Methodology, Formal analysis, Investigation, Data curation, Writing - Review and editing. **Beatriz Edith Vega Serratos:** Software, Formal analysis, Investigation, Data curation, Writing - Review and editing, Visualization. **Itxaso Oderiz Martinez:** Software, Formal analysis, Investigation, Data curation, Writing - Review and editing, Visualization. **Edgar Mendoza:** Methodology, Formal analysis, Investigation, Resources, Writing - Review and editing, Visualization, Supervision, Project administration, Funding acquisition. **Jesús María Blanco Ilzarbe:** Formal analysis, Investigation, Resources, Writing - Review and editing, Visualization, Supervision, Project administration, Funding acquisition. **Vallam Sundar:** Formal analysis, Writing - Review and editing, Visualization, Supervision. **Rodolfo Silva:** Methodology, Formal analysis, Investigation, Resources, Writing - Review and editing, Visualization, Supervision, Project administration, Funding acquisition.

Acknowledgements

The current study was conducted within the scope of CEMIE-Océano (Mexican Centre for Innovation in Ocean Energy). Project FSE-2014-06-249795 financed by CONACYT-SENER- Sustentabilidad Energética. Furthermore, the authors would like to express their gratitude to the Basque Government through the research group (IT1514/22) and are grateful for the support of Felipe Ernesto Puc Cutz and Enrique Alejandro Mangas Che in the laboratory.

References

Ahn, S., 2021. Modeling mean relation between peak period and energy period of ocean surface wave systems. Ocean Engineering 228, 108937. URL: https://www.sciencedirect.com/science/article/pii/S0029801821003723, doi:https://doi.org/10.1016/j.oceaneng.2021.108937.

Chen, J., Wen, H., Wang, Y., Wang, G., 2021. A correlation study of optimal chamber width with the relative front wall draught of onshore owc device. Energy 225, 120307. URL: https://www.sciencedirect.com/science/article/pii/S0360544221005569, doi:https://doi.org/10.1016/j.energy.2021.120307.

Daniel Raj, D., Vallam, S., Sannasiraj, S.A., 2018. Effect of harbor walls on the efficiency of an oscillating water column. Journal of Waterway, Port, Coastal, and Ocean Engineering 144, 04017043. doi:10.1061/(ASCE)WW.1943-5460.0000429.

Delmonte, N., Barater, D., Giuliani, F., Cova, P., Buticchi, G., 2016. Review of oscillating water column converters. IEEE Transactions on Industry Applications 52, 1698–1710. doi:10.1109/TIA.2015.2490629.

Durai Eswaran, S., Sannasiraj, S., Sundar, V., 2022. Experimental study on the hydrodynamic performance of an oscillating water column with frontal plates. Ocean Engineering 258, 111658. URL: https://www.sciencedirect.com/science/article/pii/S0029801822010162, doi:https://doi.org/10.1016/j.oceaneng.2022.111658.

Elhanafi, A., Fleming, A., Macfarlane, G., Leong, Z., 2016. Numerical energy balance analysis for an onshore oscillating water column–wave energy converter. Energy 116, 539–557. URL: https://www.sciencedirect.com/science/article/pii/S0360544216313901, doi:https://doi.org/10.1016/j.energy.2016.09.118.

Evans, D., Porter, R., 1995. Hydrodynamic characteristics of an oscillating water column device. Applied Ocean Research 17, 155 – 164. URL: http://www.sciencedirect.com/science/article/pii/0141118795000089, doi:https://doi.org/10.1016/0141-1187(95)00008-9.

Falcão, A.F., 2010. Wave energy utilization: A review of the technologies. Renewable and Sustainable Energy Reviews 14, 899–918. URL: https://www.sciencedirect.com/science/article/pii/S1364032109002652, doi:https://doi.org/10.1016/j.rser.2009.11.003.

Falcão, A.F., Henriques, J.C., 2014. Model-prototype similarity of oscillating-water-column wave energy converters. International Journal of Marine Energy 6, 18–34. URL: https://www.sciencedirect.com/science/article/pii/S2214166914000058, doi:https://doi.org/10.1016/j.ijome.2014.05.002.

Falcão, A.F., Henriques, J.C., 2016. Oscillating-water-column wave energy converters and air turbines: A review. Renewable Energy 85, 1391 – 1424. URL: http://www.sciencedirect.com/science/article/pii/S0960148115301828, doi:https://doi.org/10.1016/j.renene.2015.07.086.

Falcão, A.F., Henriques, J.C., 2018. The spring-like air compressibility effect in owc wave energy converters: Hydro, thermo and aerodynamic analyses. doi:10.1115/OMAE2018-77096.

Falcão, A.F., Henriques, J.C., 2019. The spring-like air compressibility effect in oscillating-water-column wave energy converters: Review and analyses. Renewable and Sustainable Energy Reviews 112, 483–498. URL: https://www.sciencedirect.com/science/article/pii/S1364032119302527, doi:https://doi.org/10.1016/j.rser.2019.04.040.

Falnes, J., 2007. A review of wave-energy extraction. Marine Structures 20, 185–201. URL: https://www.sciencedirect.com/science/article/pii/S0951833907000482, doi:https://doi.org/10.1016/j.marstruc.2007.09.001.

Fontes, J., Felix Delgado, A., Mendoza, E., Rodríguez Cueto, Y., Silva, R., 2019. On the marine energy resources of mexico. Journal of Marine Science and Engineering 7(6). doi:10.3390/jmse7060191.

Goda, Y., 2010. Random Seas and Design of Maritime Structures. 3rd ed., WORLD SCIENTIFIC. URL: https://www.worldscientific.com/doi/abs/10.1142/7425, doi:10.1142/7425, arXiv:https://www.worldscientific.com/doi/pdf/10.1142/7425.

Guedes Soares, C., Bhattacharjee, J., Tello Ruiz, M., Pietra, L., 2012. Review and classification of wave energy converters. Maritime Engineering and Technology , 585–594doi:10.1201/b12726-82.

Günther, H., Hasselmann, S., Janssen, P., 1992. The wam model cycle 4. URL: https://doi.org/10.2312/WDCC/DKRZ_Report_No04, doi:10.2312/WDCC/DKRZ_Report_No04.

He, F., Huang, Z., 2016. Using an oscillating water column structure to reduce wave reflection from a vertical wall. Journal of Waterway, Port, Coastal, and Ocean Engineering 142, 04015021. doi:10.1061/(ASCE)WW.1943-5460.0000320.

Heath, T.V., 2012. A review of oscillating water columns. Philosophical Transactions of the Royal Society A: Mathematical, Physical and Engineering Sciences 370, 235–245. doi:10.1098/rsta.2011.0164.

Henriques, J., Cândido, J., Pontes, M., Falcão, A., 2013. Wave energy resource assessment for a breakwater-integrated oscillating water column plant at porto, portugal. Energy 63, 52–60. URL: https://www.sciencedirect.com/science/article/pii/S0360544213008293, doi:https://doi.org/10.1016/j.energy.2013.09.063.

Hersbach, H., Bell, B., Berrisford, P., Hirahara, S., Horányi, A., Muñoz-Sabater, J., Nicolas, J., Peubey, C., Radu, R., Schepers, D., Simmons, A., Soci, C., Abdalla, S., Abellan, X., Balsamo, G., Bechtold, P., Biavati, G., Bidlot, J., Bonavita, M., De Chiara, G., Dahlgren, P., Dee, D., Diamantakis, M., Dragani, R., Flemming, J., Forbes, R., Fuentes, M., Geer, A., Haimberger, L., Healy, S., Hogan, R.J., Hólm, E., Janisková, M., Keeley, S., Laloyaux, P., Lopez, P., Lupu, C., Radnoti, G., de Rosnay, P., Rozum, I., Vamborg, F., Villaume, S., Thépaut, J.N., 2020. The era5 global reanalysis. Quarterly Journal of the Royal Meteorological Society 146, 1999–2049. URL: https://rmets.onlinelibrary.wiley.com/doi/abs/10.1002/qj.3803, doi:https://doi.org/10.1002/qj.3803, arXiv:https://rmets.onlinelibrary.wiley.com/doi/pdf/10.1002/qj.3803.

Howe, D., Nader, J.R., 2017. Owc wec integrated within a breakwater versus isolated: Experimental and numerical theoretical study. International Journal of Marine Energy 20, 165–182. URL: https://www.sciencedirect.com/science/article/pii/S2214166917300632, doi:https://doi.org/10.1016/j.ijome.2017.07.008.

Ibarra-Berastegi, G., Sáenz, J., Ulazia, A., Serras, P., Esnaola, G., Garcia-Soto, C., 2018. Electricity production, capacity factor, and plant efficiency index at the mutriku wave farm (2014–2016). Ocean Engineering 147, 20 – 29. URL: http://www.sciencedirect.com/science/article/pii/S0029801817306157, doi:https://doi.org/10.1016/j.oceaneng.2017.10.018.

Iturrioz, A., Guanche, R., Lara, J., Vidal, C., Losada, I., 2015. Validation of openfoam® for oscillating water column three-dimensional modeling. Ocean Engineering 107, 222–236. URL: https://www.sciencedirect.com/science/article/pii/S0029801815003649, doi:https://doi.org/10.1016/j.oceaneng.2015.07.051.

John Ashlin, S., Sannasiraj, S., Sundar, V., 2016a. Hydrodynamic performance of an array of oscillating water column device exposed to oblique waves. doi:10.13140/RG.2.2.19605.12002.

John Ashlin, S., Sannasiraj, S., Sundar, V., 2018. Performance of an array of oscillating water column devices integrated with an offshore detached breakwater. Ocean Engineering 163, 518–532. URL: https://www.sciencedirect.com/science/article/pii/S002980181830903X, doi:https://doi.org/10.1016/j.oceaneng.2018.05.043.

John Ashlin, S., Sundar, V., Sannasiraj, S., 2016b. Effects of bottom profile of an oscillating water column device on its hydrodynamic characteristics. Renewable Energy 96, 341 – 353. URL: http://www.sciencedirect.com/science/article/pii/S0960148116303937, doi:https://doi.org/10.1016/j.renene.2016.04.091.

John Ashlin, S., Sundar, V., Sannasiraj, S.A., 2017. Pressures and forces on an oscillating water column – type wave energy caisson breakwater. Journal of Waterway, Port, Coastal and Ocean Engineering 143, 1–18. doi:10.1061/(ASCE)WW.1943-5460.0000405.

Kamath, A., Bihs, H., Øivind A. Arntsen, 2015. Numerical modeling of power take-off damping in an oscillating water column device. International Journal of Marine Energy 10, 1–16. URL: https://www.sciencedirect.com/science/article/pii/S2214166915000028, doi:https://doi.org/10.1016/j.ijome.2015.01.001.

López, I., Carballo, R., Fouz, D.M., Iglesias, G., 2021. Design selection and geometry in owc wave energy converters for performance. Energies 14. doi:10.3390/en14061707.

López, I., Carballo, R., Iglesias, G., 2019. Site-specific wave energy conversion performance of an oscillating water column device. Energy Conversion and Management 195, 457–465. URL: https://www.sciencedirect.com/science/article/pii/S0196890419305771, doi:https://doi.org/10.1016/j.enconman.2019.05.030.

López, I., Carballo, R., Iglesias, G., 2020a. Intra-annual variability in the performance of an oscillating water column wave energy converter. Energy Conversion and Management 207, 112536. URL: https://www.sciencedirect.com/science/article/pii/S0196890420300728, doi:https://doi.org/10.1016/j.enconman.2020.112536.

López, I., Carballo, R., Taveira-Pinto, F., Iglesias, G., 2020b. Sensitivity of owc performance to air compressibility. Renewable Energy 145, 1334–1347. URL: https://www.sciencedirect.com/science/article/pii/S0960148119309048, doi:https://doi.org/10.1016/j.renene.2019.06.076.

López, I., Pereiras, B., Castro, F., Iglesias, G., 2014. Optimisation of turbine-induced damping for an owc wave energy converter using a rans–vof numerical model. Applied Energy 127, 105–114. URL: https://www.sciencedirect.com/science/article/pii/S0306261914003638, doi:https://doi.org/10.1016/j.apenergy.2014.04.020.

López, I., Pereiras, B., Castro, F., Iglesias, G., 2015. Performance of owc wave energy converters: influence of turbine damping and tidal variability. International Journal of Energy Research 39, 472–483. URL: https://onlinelibrary.wiley.com/doi/abs/10.1002/er.3239, doi:https://doi.org/10.1002/er.3239.

López, I., Pereiras, B., Castro, F., Iglesias, G., 2016. Holistic performance analysis and turbine-induced damping for an owc wave energy converter. Renewable Energy 85, 1155–1163. URL: https://www.sciencedirect.com/science/article/pii/S0960148115301713, doi:https://doi.org/10.1016/j.renene.2015.07.075.

Mansard, E., Funke, E., 1980. The measurement of incident and reflected spectra using a least squares method. Coastal Engineering Proceedings

1, 8. URL: https://journals.tdl.org/icce/index.php/icce/article/view/3432, doi:10.9753/icce.v17.8.

McCormick, M., 2013. Ocean Wave Energy Conversion. Dover Civil and Mechanical Engineering, Dover Publications: Mineola, NY, USA. URL: https://books.google.sc/books?id=wkDDAgAAQBAJ.

Medina Rodríguez, A.A., Blanco Ilzarbe, J.M., Silva Casarín, R., Izquierdo Ereño, U., 2020. The influence of the chamber configuration on the hydrodynamic efficiency of oscillating water column devices. Journal of Marine Science and Engineering 8. URL: https://www.mdpi.com/2077-1312/8/10/751.

Medina Rodríguez, A.A., Posada Vanegas, G., Silva Casarín, R., Mendoza Baldwin, E.G., Vega Serratos, B.E., Puc Cutz, F.E., Mangas Che, E.A., 2022. Experimental investigation of the hydrodynamic performance of land-fixed nearshore and onshore oscillating water column systems with a thick front wall. Energies 15. doi:10.3390/en15072364.

Medina Rodríguez, A.A., Silva Casarín, R., Blanco Ilzarbe, J.M., 2022. The influence of oblique waves on the hydrodynamic efficiency of an onshore owc wave energy converter. Renewable Energy 183, 687–707. URL: https://www.sciencedirect.com/science/article/pii/S0960148121016426, doi:https://doi.org/10.1016/j.renene.2021.11.061.

Meinert, P., Andersen, T.L., Frigaard, P., 2017. AwaSys 7 user manual. URL: http://homes.civil.aau.dk/tla/awasys/downloads/AwaSys7UserManual.pdf.

Morris-Thomas, M.T., Irvin, R.J., Thiagarajan, K.P., 2006. An Investigation Into the Hydrodynamic Efficiency of an Oscillating Water Column. Journal of Offshore Mechanics and Arctic Engineering 129, 273–278. URL: https://doi.org/10.1115/1.2426992, doi:10.1115/1.2426992, arXiv:https://asmedigitalcollection.asme.org/offshoremechanics/article-pdf/129/4/273/5810589/273_1.pdf.

Ning, D.Z., Wang, R.Q., Zou, Q.P., Teng, B., 2016. An experimental investigation of hydrodynamics of a fixed owc wave energy converter. Applied Energy 168, 636 – 648. URL: http://www.sciencedirect.com/science/article/pii/S0306261916300952, doi:https://doi.org/10.1016/j.apenergy.2016.01.107.

Odériz, I., Silva, R., Mortlock, T., Mendoza, E., 2020. Climate drivers of directional wave power on the mexican coast. Ocean Dynamics 70. doi:10.1007/s10236-020-01387-z.

Orphin, J., Schmitt, P., Nader, J.R., Penesis, I., 2022. Experimental investigation into laboratory effects of an owc wave energy converter. Renewable Energy 186, 250–263. URL: https://www.sciencedirect.com/science/article/pii/S096014812101819X, doi:https://doi.org/10.1016/j.renene.2021.12.092.

Payne, G., 2008. Guidance for the Experimental Tank Testing of Wave Energy Converters. SuperGen Marine, University of Strathclyde: Glasgow, UK.

Quintero-Nuñez, M., Sweedler, A., Tanaka, S., 2006. Renewable resources of energy in northern baja california, mexico, pp. 769–778. doi:10.2495/RAV060751.

Rezanejad, K., Guedes Soares, C., López, I., Carballo, R., 2017. Experimental and numerical investigation of the hydrodynamic performance of an oscillating water column wave energy converter. Renewable Energy 106, 1 – 16. URL: http://www.sciencedirect.com/science/article/pii/S0960148117300034, doi:https://doi.org/10.1016/j.renene.2017.01.003.

Ringwood, J.V., 2020. Wave energy control: status and perspectives 2020 ∗∗this paper is based upon work supported by science foundation ireland under grant no. 13/ia/1886 and grant no. 12/rc/2302 for the marine renewable ireland (marei) centre. IFAC-PapersOnLine 53, 12271–12282. URL: https://www.sciencedirect.com/science/article/pii/S2405896320315536, doi:https://doi.org/10.1016/j.ifacol.2020.12.1162. 21st IFAC World Congress.

Sarmento, A., 1993. Model-Test Optimization Of An Owc Wave Power Plant. International Journal of Offshore and Polar Engineering 3.

Sundar, V., Moan, T., Todalshaug, J., 2010. Conceptual design of owc wave energy converters combined with breakwater structures. Proceedings of the International Conference on Offshore Mechanics and Arctic Engineering - OMAE 3, 479–489. doi:10.1115/OMAE2010-20508.

Terrero González, A., Dunning, P., Howard, I., McKee, K., Wiercigroch, M., 2021. Is wave energy untapped potential? International Journal of Mechanical Sciences 205, 106544. URL: https://www.sciencedirect.com/science/article/pii/S0020740321002794, doi:https://doi.org/10.1016/j.ijmecsci.2021.106544.

Torre-Enciso, Y., Ortubia, I., Aguileta, L., Marqués, J., 2009. Mutriku wave power plant: From the thinking out to the reality. Proceedings of the 8th European Wave and Tidal Energy Conference , 319–329.

Tsai, C.P., Ko, C.H., Chen, Y.C., 2018. Investigation on performance of a modified breakwater-integrated owc wave energy converter. Sustainability 10. doi:10.3390/su10030643.

Ventura, Y., Rodríguez, Y., Odériz, I., Chávez, V., Mori, N., Felix, A., Cerdeira-Estrada, S., Silva, R., 2022. New assessment of wave energy in relation to geomorphological and demographic characteristics on the pacific coast of baja california, mexico. Frontiers in Marine Science 9. URL: https://www.frontiersin.org/articles/10.3389/fmars.2022.872707, doi:10.3389/fmars.2022.872707.

Viviano, A., Naty, S., Foti, E., 2018. Scale effects in physical modelling of a generalized owc. Ocean Engineering 162, 248–258. URL: https://www.sciencedirect.com/science/article/pii/S0029801818307777, doi:https://doi.org/10.1016/j.oceaneng.2018.05.019.

Viviano, A., Naty, S., Foti, E., Bruce, T., Allsop, W., Vicinanza, D., 2016. Large-scale experiments on the behaviour of a generalised oscillating water column under random waves. Renewable Energy 99, 875 – 887. URL: http://www.sciencedirect.com/science/article/pii/S0960148116306826, doi:https://doi.org/10.1016/j.renene.2016.07.067.

Wang, R.Q., Ning, D.Z., Zhang, C.W., Zou, Q.P., Liu, Z., 2018. Nonlinear and viscous effects on the hydrodynamic performance of a fixed owc wave energy converter. Coastal Engineering 131, 42 – 50. URL: http://www.sciencedirect.com/science/article/pii/S0378383917300637, doi:https://doi.org/10.1016/j.coastaleng.2017.10.012.

Çelik, A., Altunkaynak, A., 2020. Determination of hydrodynamic parameters of a fixed owc by performing experimental and numerical free decay tests. Ocean Engineering 204, 106827. URL: https://www.sciencedirect.com/science/article/pii/S0029801819309254, doi:https://doi.org/10.1016/j.oceaneng.2019.106827.